© 2016. Published by The Company of Biologists Ltd | Journal of Cell Science (2016) 129, 367-379 doi:10.1242/jcs.176651

RESEARCH ARTICLE

Srv2/CAP is required for polarized actin cable assembly and patch internalization during clathrin-mediated endocytosis

Junko Y. Toshima[1,2,*], Chika Horikomi[3,*], Asuka Okada[3,*], Makiko N. Hatori[3], Makoto Nagano[2], Atsushi Masuda[3], Wataru Yamamoto[3], Daria Elisabeth Siekhaus[4] and Jiro Toshima[2,3,‡]

ABSTRACT

The dynamic assembly and disassembly of actin filaments is essential for the formation and transport of vesicles during endocytosis. In yeast, two types of actin structures, namely cortical patches and cytoplasmic cables, play a direct role in endocytosis, but how their interaction is regulated remains unclear. Here, we show that Srv2/CAP, an evolutionarily conserved actin regulator, is required for efficient endocytosis owing to its role in the formation of the actin patches that aid initial vesicle invagination and of the actin cables that these move along. Deletion of the *SRV2* gene resulted in the appearance of aberrant fragmented actin cables that frequently moved past actin patches, the sites of endocytosis. We find that the C-terminal CARP domain of Srv2p is vitally important for the proper assembly of actin patches and cables; we also demonstrate that the N-terminal helical folded domain of Srv2 is required for its localization to actin patches, specifically to the ADP-actin rich region through an interaction with cofilin. These results demonstrate the *in vivo* roles of Srv2p in the regulation of the actin cytoskeleton during clathrin-mediated endocytosis.

KEY WORDS: Srv2, CAP, Actin, Cofilin, Endocytosis

INTRODUCTION

The coordinated regulation of the assembly and disassembly of actin filaments is required for various cellular functions, including the formation and internalization of endocytic vesicles (Goode et al., 2015; Kaksonen et al., 2006; Perrais and Merrifield, 2005). In yeast, the actin cytoskeleton exists in three distinct types of structure: cortical patches, cables and the contractile ring (Moseley and Goode, 2006). The actin cortical patches are a dense dendritic network of actin filaments that are assembled at endocytic sites (Goode et al., 2015; Kaksonen et al., 2006; Winter et al., 1997). Actin cables are bundles of actin filaments that generally align with the long axis of the cell, and serve as tracks for vesicle transport and organelle segregation (Bretscher, 2003; Yang and Pon, 2002). A previous study that used three-dimensional imaging has demonstrated that actin cables attach both at their ends and laterally to cortical patches (Amberg, 1998). We and other groups have also shown previously that actin patches (clathrin-coated vesicles, CCVs) associate with and move toward early endosomes along actin cables after being internalized into the cytosol (Huckaba et al., 2004; Toshima et al., 2006), suggesting that actin cables might function as tracks to transport CCVs to early endosomes. Although evidence increasingly indicates a functional connection between actin patches and cables, the timing of their interaction and the molecular machinery tethering CCVs to actin cables are still poorly understood.

Actin disassembly during endocytosis in yeast is driven by the coordinated activities of multiple actin-binding proteins, such as Cof1p (yeast cofilin), Crn1p (yeast coronin), Aip1p (actin-interacting protein 1), and Srv2/cyclase-associated protein (CAP) (Goode et al., 2015). All of these proteins are components of the actin cytoskeleton that are widely conserved among eukaryotes. Cof1p binds to the sides of actin filaments and severs the filaments with the help of Aip1p or Crn1p (Jansen et al., 2015). Activities of Srv2p with Cof1p also promote actin filament disassembly *in vitro* (Balcer et al., 2003; Moriyama and Yahara, 2002). The timing of the localization of Srv2p to actin patches during endocytosis has not been investigated. Cof1p, Crn1p and Aip1p appear at actin patches about 5 s later than Abp1p, and are lost from the patches later than Abp1p (Lin et al., 2010; Okreglak and Drubin, 2007). A study by Lin et al. has revealed that Cof1p assembles at a time point when the initial movement of the cortical patches had already begun and that the actin patches keep moving as they accumulate Cof1p (Lin et al., 2010). Thus, Cof1p and its interacting proteins seem to function in the later stages of endocytic internalization.

Srv2p, also called cyclase-associated protein (CAP), is a highly conserved actin-binding protein that is required for normal actin organization in organisms ranging from yeast to mammals (Ono, 2013). Srv2p has several motifs and domains, including an N-terminal oligomerization domain, a dimeric helical folded domain (HFD) and a Wasp homology 2 (WH2) domain, which are sandwiched between two poly-proline (P1 and P2) motifs, and a dimeric folded domain termed the CARP domain, entirely comprising β-sheets, at the C-terminus (Ono, 2013). The function of Srv2p in actin turnover has been established in several excellent biochemical studies. The C-terminal region of Srv2p has a role in G-actin nucleotide exchange, and also in the recycling of cofilin, a ubiquitously expressed actin depolymerization factor. These functions are accomplished through a high-affinity association of the Srv2p C-terminus with ADP-G-actin, which releases the actin from cofilin (Balcer et al., 2003; Balderhaar et al., 2013; Chaudhry et al., 2010; Mattila et al., 2004; Moriyama and Yahara, 2002). By contrast, the N-terminal oligomerization and the HFD domains can catalyze cofilin-mediated severing of actin filaments (Chaudhry et al., 2013; Jansen et al., 2014). In addition, several proteins have been reported to selectively bind to either the P1 or P2 regions of Srv2p; profilin, a nucleotide exchange factor for actin, binds to P1 (Bertling et al., 2007), and Abp1p, an actin-binding protein, binds to P2 (Freeman et al., 1996; Lila and Drubin, 1997). Although these

[1]Department of Liberal Arts, Tokyo University of Technology, 5-23-22 Nishikamada, Ota-ku, Tokyo 144-8535, Japan. [2]Research Center for RNA Science, RIST, Tokyo University of Science, 6-3-1 Niijyuku, Katsushika-ku, Tokyo 125-8585, Japan. [3]Department of Biological Science and Technology, Tokyo University of Science, 6-3-1 Niijyuku, Katsushika-ku, Tokyo 125-8585, Japan. [4]Institute of Science and Technology Austria, Am Campus 1, Klosterneuburg A-3400, Austria.
*These authors contributed equally to this work

‡Author for correspondence (jtosiscb@rs.noda.tus.ac.jp)

Received 30 June 2015; Accepted 19 November 2015

Journal of Cell Science (2016) 129, 367-379 doi:10.1242/jcs.176651

studies provide a potential framework for understanding how Srv2p and its binding proteins regulate the assembly and disassembly of actin filaments *in vitro*, the physiological role of Srv2p in the formation of actin patches and/or cables has still remained unclear.

In the present study, we screened yeast strains carrying single-gene deletion mutations for defects in actin cable formation and dynamics, and identified *SRV2* as such a gene. We also demonstrated that the *srv2*Δ mutant exhibits severely defective actin patch disassembly and endocytic internalization. Furthermore, we analyzed several domain-deletion and point mutants of Srv2p, and show the functional regions of Srv2p that are required for the proper assembly and disassembly of actin patches and cables. These data indicate that there are multiple *in vivo* roles for Srv2p in the regulation of the actin cytoskeleton that are required for normal endocytosis.

RESULTS

Quantitative phenotypic analysis of yeast deletion mutants defective in actin cable assembly

Previous studies have demonstrated that internalization of actin patches is mediated by polarized actin cables (Huckaba et al., 2004; Kaksonen et al., 2003; Toshima et al., 2006). However, how actin patches and cables cooperate to drive the formation and internalization of endocytic vesicles has not been clarified. To help us study these processes, we characterized Abp140p that had been fused with three tandem copies of GFP (3GFP) to confirm that Abp140–3GFP can serve as a marker of both actin patches and actin cables. Consistent with a previous observation, most Apb140p-labeled actin patches (>98%) were found to colocalize with patches that were labeled by Abp1–mCherry, a widely used actin patch marker (Fig. S1A and Movie 1) (Toshima et al., 2006). We also found that the timing of Abp140p recruitment to cortical patches, and the lifetimes and dynamics of Abp140p patches, were almost the same as those of Abp1p patches (Fig. S1B–E). From these results, we concluded that Abp140–3GFP can serve as a marker for both actin cables and patches. We then sought to identify the proteins required for actin cable assembly at endocytic sites. We selected 19 genes that have been reported to be related to actin patch assembly in yeast (Engqvist-Goldstein and Drubin, 2003; Moseley and Goode, 2006) and expressed Abp140–3GFP as a marker for actin cables (Yang and Pon, 2002) in cells that lacked each of the individual genes (Fig. 1A). Among the 19 mutants examined, five mutants – *bni1-12 bnr1*Δ, *cap1*Δ, *cap2*Δ, *sac6*Δ and *srv2*Δ – showed prominent localization of Abp140–3GFP at actin patches (Fig. 1A; Movie 2). Quantitative analysis revealed that the levels of actin patch fluorescence in these five mutants were remarkably increased

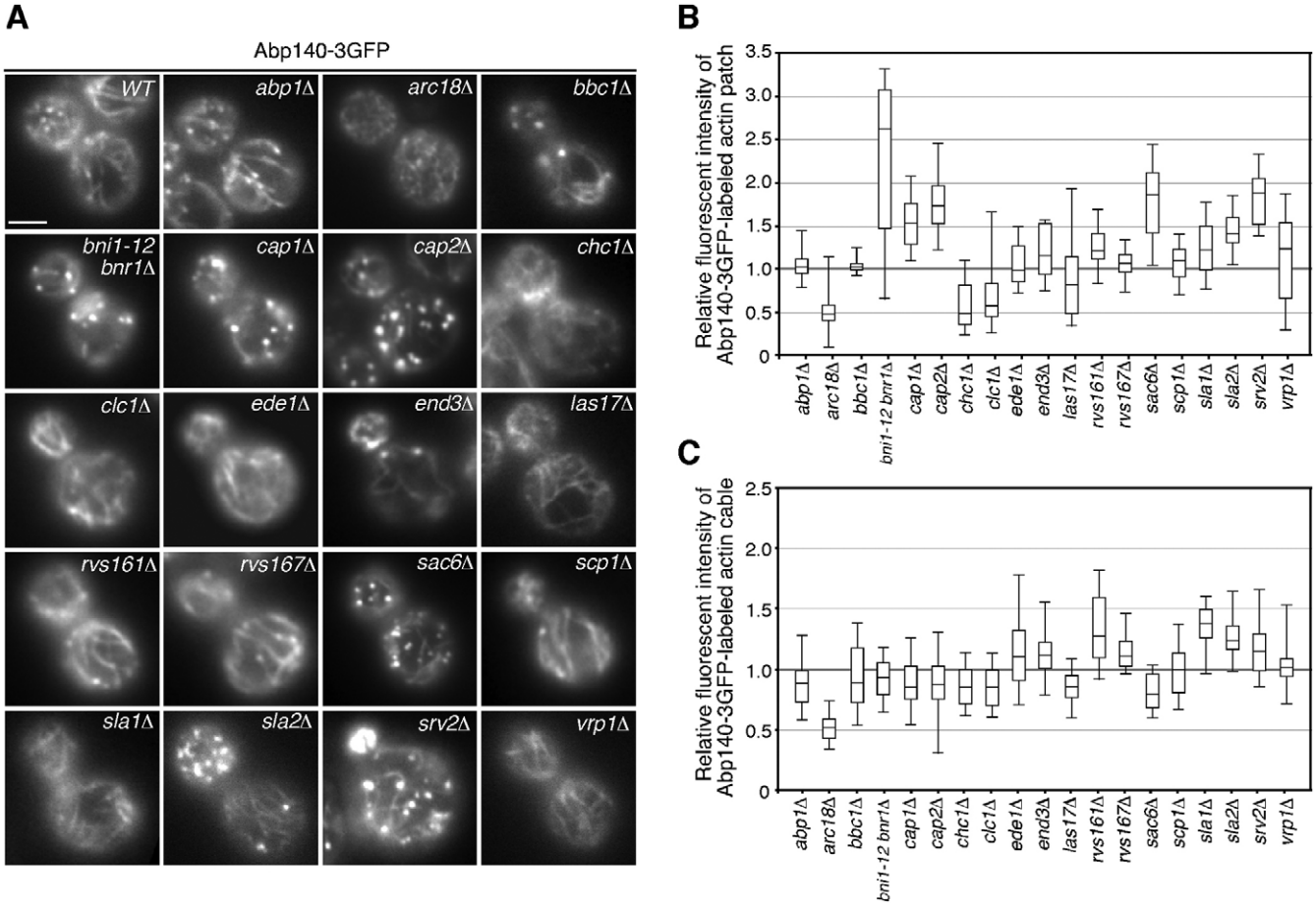

Fig. 1. Localization of actin cables and patches in different mutant cells. (A) Localization of Abp140–3GFP in different mutant cells. Cells expressing Abp140–3GFP were grown to early- to mid-logarithmic phase in YPD medium at 25°C and observed by using fluorescence microscopy. Scale bar: 2.5 µm. (B) Quantification of the fluorescence intensity of Abp140–3GFP-labeled actin patches in each mutant cell. The relative fluorescence intensity of cortical patches was calculated as described in the Materials and Methods. Charts show box plots of the data (n=50 patches for each cell). The line indicates the median, the edges of the box indicate the 25 and 75% percentiles, and the whiskers extend to the extremes of the data. (C) Quantification of the fluorescence intensity of Abp140-3GFP-labeled actin cables in each mutant cell. The relative fluorescence intensity of actin cables was calculated as described in the Materials and Methods. Charts show box plots of the data (n=50 cables for each cell), as described in B.

Journal of Cell Science (2016) 129, 367-379 doi:10.1242/jcs.176651

(>1.5 fold), relative to that in wild-type cells, in all of these mutants (Fig. 1B). In contrast, the fluorescence intensity of actin cables was decreased in the *bni1-12 bnr1*Δ, *cap1*Δ, *cap2*Δ and *sac6*Δ mutants (Fig. 1A,C). Similar phenotypes have been reported previously for *cap1*Δ, *cap2*Δ and *sac6*Δ mutants (Adams et al., 1991; Amatruda and Cooper, 1992; Kim et al., 2004). The yeast formin mutant (*bni1-12 bnr1*Δ) displayed a decreased intensity of actin cable fluorescence, as described previously (Evangelista et al., 2002; Sagot et al., 2002). Aberrant actin structures in the *srv2*Δ mutant have been reported in previous studies (Chaudhry et al., 2013, 2010). Consistent with previous studies, the *srv2*Δ mutant showed highly depolarized actin patches, and disorganized and partially diminished actin cables (Fig. 1A). In the *srv2*Δ mutant, the fluorescence intensity of actin patches was markedly increased (Fig. 1B), suggesting that excessive actin polymerization might occur at cortical patches. In contrast, the fluorescence intensity of actin cables was not significantly altered, although many of the actin cables were fragmented (Fig. 1A,C). Interestingly, the dynamics of the fragmented short actin cables were quite unique and never observed in other mutants (Fig. 1A; Movie 2).

Spatio-temporal analysis of actin cable recruitment to cortical patches

As shown previously, over 85% of actin patches, even in single focal plane images, were found to associate with actin cables during internalization (see Fig. 2I). However, as the precise timing of actin cable recruitment to cortical patches has not been determined, we next investigated the spatio-temporal dynamics of actin patches and actin cables at endocytic sites. Live-cell imaging using cells expressing Abp140–3GFP showed that some actin cables were recruited to cortical patches before actin patch formation, whereas others were recruited thereafter (Fig. S2A,B; Movie 3). Quantitative analysis to categorize actin cable recruitment as occurring before, after or simultaneously with actin patch formation revealed that approximately 39% of actin cables were recruited after actin patch formation, whereas around

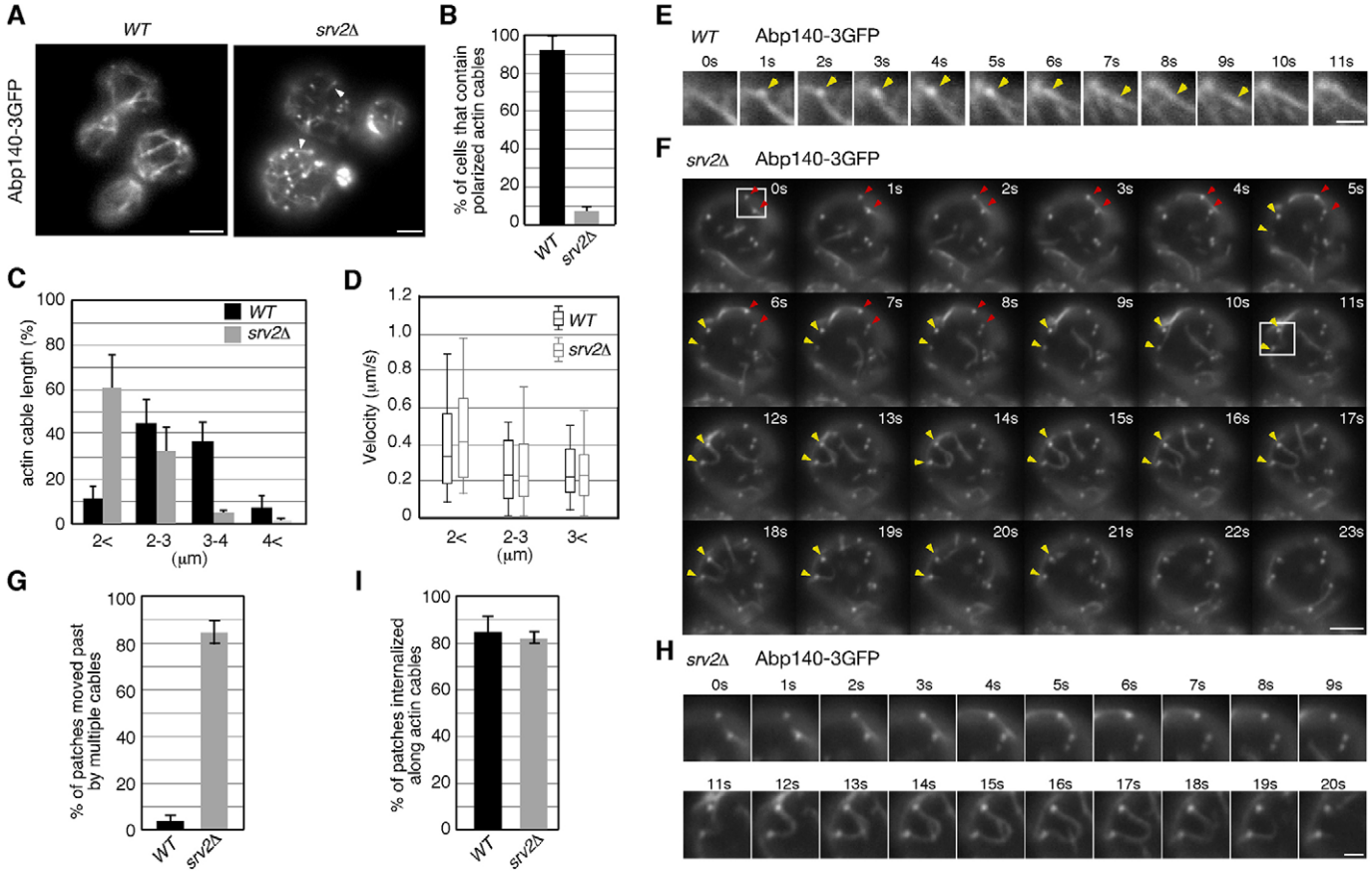

Fig. 2. Actin cable dynamics in the *srv2*Δ mutant. (A) Localization of Abp140–3GFP in wild-type (WT) and *srv2*Δ cells. Scale bars: 2.5 µm. (B) Actin cable polarization is disrupted in *srv2*Δ cells. The bar graphs represent the percentage of cells that contained polarized actin cables in wild-type and *srv2*Δ cells (*n*=100 cells for each strain). (C) Quantification of the length of actin cables in wild-type and *srv2*Δ cells. To determine the length of actin cables accurately, actin cables whose lengths did not change for at least 3 frames (>3 s) during the time-lapse imaging were selected and measured by using the program ImageJ v1.44. Data show the mean±s.d., *n*=50 cables for each strain. (D) The velocity of Abp140–GFP-labeled cable movement categorized by the cable length. To determine the velocity of >3 µm actin cables, the distance traveled in 1.0 s by the center of the bright fluorescent regions ('fiduciary marks'; Yang and Pon, 2002) was calculated based on pixel coordinates (1 pixel=64.5 nm). To determine the velocities of <2-µm and 2–3-µm actin cables, the distance traveled in 1.0 s by the leading edge of fragmented actin cables was calculated. Charts show box plots of the data, as described for Fig. 1B. (E) The localization of Abp140–3GFP-labeled patches and cables in wild-type cells. Arrowheads indicate examples of an actin patch internalized along an actin cable. Scale bar: 1.0 µm. (F) Localization of Abp140–3GFP-labeled patches and cables in *srv2*Δ cells. Arrowheads indicate examples of actin patches with which an actin cable associated and then passed by. Scale bar: 2.5 µm. (G) The bar graphs represent the percentage of actin patches that were passed by more than two different actin cables in a 2-min period of time-lapse imaging. Data are mean±s.d. from at least three experiments, with >50 patches counted for each strain per experiment. (H) High-magnification views of the boxed areas shown in F. Scale bar: 1.0 µm. (I) The bar graphs represent the percentage of patches internalized along actin cables in wild-type or *srv2*Δ cells. Data are means±s.d. from at least three experiments, with >50 patches counted for each strain per experiment.

Journal of Cell Science (2016) 129, 367-379 doi:10.1242/jcs.176651

48% were recruited beforehand in wild-type cells (Fig. S2C). Similar analysis was performed for the deletion mutants, except for *sla2*Δ in which severely defective actin patch formation has been observed (Kaksonen et al., 2003). The proportion of actin cables recruited after actin patch formation was markedly increased (>60%) in the *bni1-12 bnr1*Δ, *cap1*Δ, *cap2*Δ and *srv2*Δ mutants (Fig. S2C). As shown in Fig. 1B, all of these mutants exhibited increased intensity of actin patch fluorescence. Among these mutants, *srv2*Δ exhibited the most intriguing phenotypic change in actin cable dynamics, and therefore became the mutant that we decided to focus our analysis on.

Aberrant actin cable dynamics in the *srv2*Δ mutant

Srv2p has been demonstrated to be part of a multimeric complex that recycles actin monomers from ADF and cofilin, making them available for new rounds of filament assembly (Goode et al., 2015; Ono, 2013). In wild-type cells, actin cables showed a polarized alignment, extending from the bud neck towards the opposite tip, parallel to the longitudinal axis of the cell (Fig. 2A). In contrast, in the *srv2*Δ mutant, these polarized actin cables were observed much less frequently than in wild-type cells (7.2% and 92.5%, respectively) (Fig. 2B), and fragmented short actin cables oriented in random directions were more evident (Fig. 2A, arrowheads). Quantitative analysis of actin cable lengths revealed that the number of short actin cables (<2 µm) was significantly increased in *srv2*Δ cells relative to wild-type cells (Fig. 2C,D). Short actin cables move faster than long ones, yet the velocities of actin cables were almost the same between wild-type and *srv2*Δ cells when cables of the same length were compared to one another (Fig. 2D). We next examined the dynamics of actin cables at cortical patches in the *srv2*Δ mutant. In wild-type cells, we observed that actin patches invariably associate with actin cables and are then lost (Fig. 2E), as reported previously (Huckaba et al., 2004; Toshima et al., 2006). In the *srv2*Δ mutant, however, we found that actin cables were directed to pre-existing actin patches, became associated with them and then moved away from them (Fig. 2F, red arrowheads; Movie 4). In this mutant, we also found that multiple actin cables moved past a single actin patch (Fig. 2G). Such events were observed frequently only in *srv2*Δ cells (~85.5%) and were rare in wild-type cells (<5%) (Fig. 2G). Additionally, we detected one actin cable that sequentially moved past two different actin patches located close to each other (Fig. 2F, yellow arrowheads, 2H, upper panels; Movie 4). Interestingly, actin cables occasionally exhibited a curved structure when simultaneously moving past two patches, indicating that, in the *srv2*Δ, mutant actin cables can attach to multiple actin patches at the same time and that one attachment is fixed and the other isn't, resulting in the curve. Although internalization events occurred less frequently in the *srv2*Δ mutant, over 80% of actin patches were internalized along actin cables at the internalization step of endocytosis, similar to the situation in wild-type cells (Fig. 2I). These observations suggest that, in the *srv2*Δ mutant, short actin cables are regularly recruited to sites of actin patch assembly but that tethering of endocytic vesicles on actin cables is defective.

Disruption of actin patch dynamics and endocytic internalization in *srv2*Δ cells

Previous studies have indicated that deletion of the *SRV2* gene does not result in changes in endocytosis-related parameters, such as the internalization of radiolabeled α-factor and the lifetimes of endocytic proteins (Kaksonen et al., 2005; Wesp et al., 1997). To confirm this, we next examined the effect of the deletion of *SRV2* on endocytosis by assessing the internalization and transport of Alexa-Fluor-594-labeled α-factor (A594-α-factor) (Toshima et al., 2014). We examined the localization of A594-α-factor at several time points after its addition to wild-type and *srv2*Δ cells. In wild-type cells, the majority of A594-α-factor had been transported to the vacuole 15 min after addition (Fig. 3A). In contrast, an obvious delay of A594-α-factor internalization was observed in the *srv2*Δ mutant (Fig. 3A). Quantitative analyses revealed that the fluorescence intensity of A594-α-factor decreased to ~20% in wild-type cells at 5 min after α-factor addition, and the fluorescence was mostly lost after 15 min, whereas approximately 61% and 26% of A594-α-factor remained at the plasma membrane in *srv2*Δ cells after 15 and 30 min, respectively (Fig. 3B). We further examined the effect on endocytosis by assessing the internalization of ^{35}S-labeled α-factor. In contrast to a previous observation (Wesp et al., 1997), we found that *srv2*Δ cells exhibited a marked defect in ^{35}S-labeled α-factor internalization (Fig. 3C). We also examined the effect of *SRV2* deletion on recycling of the plasma membrane vesicle (v-)SNARE Snc1p, a plasma-membrane-recycling marker in yeast (Gurunathan et al., 2000). Consistent with A594-α-factor internalization, we found that recycling of Snc1p was impaired at the stage of endocytic internalization, whereas transport of Snc1p to the plasma membrane seemed to be normal (Fig. 3D). Furthermore, we found that binding of ^{35}S-labeled α-factor to the cell surface was almost the same between wild-type and *srv2*Δ cells (Fig. 3E). These results suggest that the expression level of the α-factor receptor on the cell surface does not differ between wild-type and *srv2*Δ cells, and that *srv2*Δ cells have a defect in the internalization step of endocytosis.

We next examined whether the dynamics of the late coat module and actin patch were affected in the *srv2*Δ mutant. In contrast to previous studies, the lifetime of Sla1–GFP, a marker of the late clathrin coat, was significantly increased in the *srv2*Δ mutant (141±66 s; mean±s.d.), compared to that of wild-type cells (29±6 s) (Fig. 3F,G). Two-color simultaneous imaging revealed that Sla1–GFP was internalized at the same time as Abp1–mCherry (Fig. 3F; Movie 5). Similar to Sla1p, the lifetime of Abp1p was considerably increased in the *srv2*Δ mutant, relative to that in wild-type cells (43±11 and 16±5 s, respectively) (Fig. 3F,H). Quantification of the fluorescence intensity for individual Abp1p patches showed that the time required to reach the maximum fluorescence intensity and the time required to decrease to the minimum intensity were both markedly increased in the mutant (Fig. 3I). Furthermore, the tracking of individual patches showed that the distance and time of the migration that patches engaged in after being released from the plasma membrane were increased in the *srv2*Δ mutant (Fig. 3J,K). These results suggest that the *srv2*Δ mutants have a defect in both the assembly and disassembly of actin patches, resulting in a severe defect in endocytic internalization.

Effects of Srv2p domain deletion on actin and endocytic vesicle formation

To investigate in more detail the role of Srv2p on actin-mediated endocytosis, we created Srv2 mutants in which different portions of the protein were deleted, either the HFD domain (ΔHFD), the WH2 and two proline-rich motifs (ΔPWP), or the C-terminal CARP domain (ΔCARP). Each mutation was integrated into the endogenous *SRV2* locus (Fig. 4A), replacing the original gene. We also did this with the full-length *SRV2* gene, putting it back into the endogenous locus in the *srv2*Δ mutant to confirm the functionality of this approach. These three mutant cell lines showed fewer polarized actin cables and increased Abp1p lifetimes, compared to wild-type cells (Fig. 4B–D). In contrast, cells into which the full-length *SRV2* gene had been integrated

Journal of Cell Science

Journal of Cell Science (2016) 129, 367-379 doi:10.1242/jcs.176651

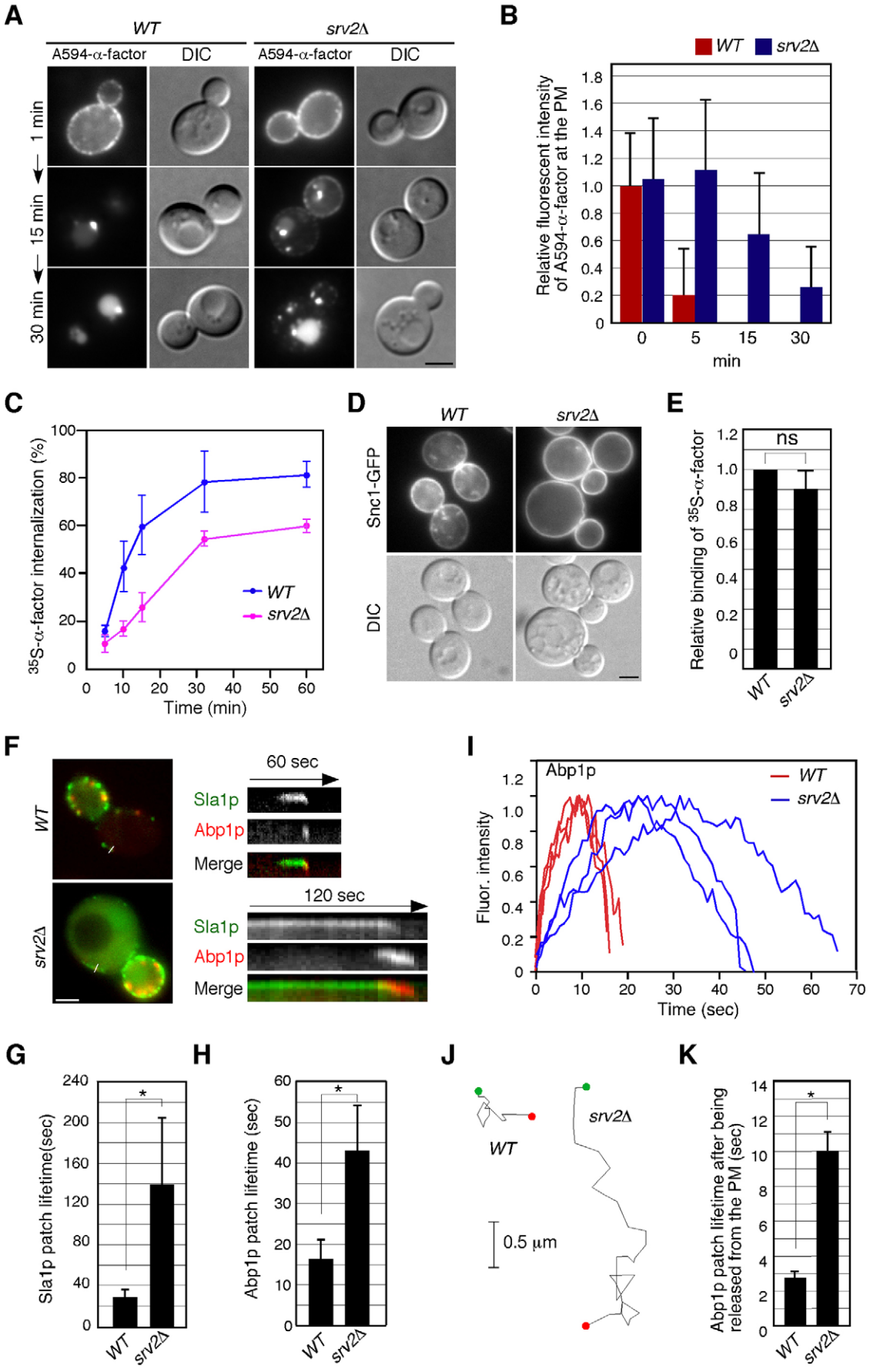

Fig. 3. See next page for legend.

Journal of Cell Science (2016) 129, 367-379 doi:10.1242/jcs.176651

Fig. 3. Dynamics of actin patches in *srv2*Δ mutants. (A) Wild-type (WT) and *srv2*Δ cells were labeled with A594-α-factor, as described in the Materials and Methods. The images were acquired at 0, 15 and 30 min after washing out unbound A594-α-factor and warming the cells to 25°C. DIC, differential interference contrast. (B) Quantification of the localization of A594-α-factor in wild-type and *srv2*Δ cells. The average fluorescence intensities of A594-α-factor at the plasma membrane were calculated by averaging the fluorescence intensities of at least 50 randomly selected areas (1×1 pixel area) in the plasma membrane. To calculate the membrane-associated fluorescence of A594-α-factor, the average fluorescence intensity of the plasma membrane was subtracted from the average cytosolic fluorescence intensity. The bar graphs represent the relative fluorescence intensity of the A594-α-factor remaining at the plasma membrane at the indicated times after internalization. Data are the means±s.d. from at least three experiments. (C) Internalization of radiolabeled α-factor in wild-type and *srv2*Δ cells at 25°C. Each curve represents the average of four independent experiments, and error bars indicate the s.d. at each time point. (D) Localization of Snc1–GFP in wild-type and *srv2*Δ cells. (E) The relative amount of ^{35}S-labeled α-factor bound to wild-type and *srv2*Δ cells. Error bars represent the s.d. from at least three experiments. ns, not significant, unpaired Student's *t*-test. (F) The localization of Sla1–GFP and Abp1–mCherry in live cells is shown in the left-hand panels. Lines in the image mark where the kymograph in the right-hand panels was generated. All movies were taken with a 1-s frame interval for both Sla1–GFP and Abp1–mCherry. (G) Average lifetimes of Sla1–GFP±s.d. for indicated strains. Data were taken from 1-min movies with a 1-s frame interval for wild-type cells, and 4-min movies with a 3-s frame interval for *srv2*Δ cells. *n*=50 patches for each strain. **P*<0.001, unpaired *t*-test. (H) Average lifetimes of Abp1–mCherry±s.d. in wild-type and *srv2*Δ cells. Data were taken from a 2-min movie with a 1-s frame interval. *n*=50 patches for each strain. **P*<0.001, unpaired Student's *t*-test. (I) Quantification of the fluorescence intensity of Abp1–mCherry in wild-type (red) and *srv2*Δ (blue) cells. Each curve represents data from one patch. The behavior of three independent patches was plotted for each strain. (J) Tracking of individual cortical Abp1p patches. Abp1–mCherry was observed every 1 s, and patch movement traces were obtained for the entire lifetime of the patches. Green and red dots indicate the first and last position, respectively. (K) Average lifetimes of Abp1–mCherry patches after they are released from the plasma membrane. *n*=50 patches for each strain. **P*<0.001, unpaired Student's *t*-test. Scale bars: 2.5 µm.

exhibited normal actin structures, similar to wild-type cells (Fig. 4B–D). Quantitative analyses revealed that *srv2ΔCARP* cells mostly, and *srv2ΔHFD* and *srv2ΔPWP* cells partially lacked polarized actin patches and cables, corresponding to the growth phenotype (Fig. 4C; Fig. S3A). The lifetime of Abp1p patches was considerably increased in *srv2ΔCARP* cells (~35±12 s; mean±s.d.), whereas *srv2ΔHFD* and *srv2ΔPWP* cells exhibited a moderate increase (~28±7 and 24±5 s, respectively) (Fig. 4D). These results suggest that the CARP domain has a more important role in endocytic vesicle formation. Particle-tracking analysis revealed that in *srv2ΔHFD* and *srv2ΔPWP* cells, relative to wild-type cells, the time taken for actin patches to reach maximum fluorescence intensity was not significantly altered, but the time required for the fluorescence intensity to decrease was longer (Fig. 4E). This suggests that deletion of the HFD and PWP domains primarily affects disassembly of actin patches. In contrast, in *srv2ΔCARP* cells, the times required for the fluorescence intensity to both increase and decrease were longer (Fig. 4E), indicating a requirement of the CARP domain for both assembly and disassembly of actin patches.

Abp1p-independent localization of Srv2p at cortical actin patches

We wished to determine whether any of the changes in actin behavior that we observed in the Srv2p domain mutants were due to changes in the localization of the protein. A previous indirect immunofluorescence study has demonstrated that Srv2p colocalizes with cortical actin patches and that binding of poly-proline motifs to Abp1p are required for this localization (Freeman et al., 1996; Lila and Drubin, 1997; Yu et al., 1999). To perform an in-depth characterization of the localization and dynamics of Srv2p, we tagged Srv2p and its domain-deletion mutants with GFP, and examined their localization in living cells. Western blotting analysis using an antibody against GFP confirmed that each gene product was expressed with the correct molecular mass in each mutant cell (Fig. 5A). Live-cell imaging revealed that Srv2–GFP patches formed at the cell cortex with a lifetime of 11±4 s (mean±s.d.), culminating in inward movement (Fig. 5B,C; Movie 6). Srv2p patches had similar dynamics to actin patches, initially appearing as a stationary patch and then undergoing rapid inward movement away from the original position before being lost in the cytoplasm (Fig. 5D). We also examined the localization of Srv2p domain-deletion mutants and found that deletion of the PWP domain significantly decreased Srv2p localization at cortical patches (Fig. 5B,F), consistent with previous observations (Lila and Drubin, 1997; Yu et al., 1999). The localization of Srv2ΔHFD and Srv2ΔCARP at cortical patches slightly decreased compared to that of full-length Srv2p, whereas the mean lifetimes were increased (24±1 s and 27±2 s, respectively) (Fig. 5B,C,F). Unexpectedly, the fluorescence intensity of the cortical patches of GFP-tagged Srv2ΔHFD protein was increased about 1.6-fold compared to that of full-length Srv2p (Fig. 5B,G). Interestingly, the fluorescence intensity of Abp1p patches was similarly increased in *srv2ΔHFD* cells (Fig. 5G), suggesting that the loss of the F-actin-disassembly-promoting activity of HFD probably causes an increase of F-actin in the patches. Because it has been reported that Abp1p has a role in the localization of Srv2p (Freeman et al., 1996), we next examined whether the localization of each deletion mutant depends on the presence of Abp1p. The Srv2p cortical localization was affected by deleting the *ABP1* gene, consistent with the findings of an earlier report, but the average number of Srv2ΔPWP patches in *abp1*Δ cells was almost the same as that of Srv2p patches in the *srv2ΔPWP* cells (Fig. 5E,F). Intriguingly, we found that deletion of the HFD or CARP domain of Srv2p further decreased the cortical localization of Srv2p when expressed in *abp1*Δ cells (Fig. 5E,F). These observations suggest that Srv2p localization at cortical patches is dependent on other interactions that are mediated by the HFD and CARP domains, in addition to interactions with Abp1p through the PWP region.

To determine the timing of Srv2p recruitment to actin patches, we performed simultaneous two-color imaging of Srv2–GFP and Abp1–mCherry (Movie 6). In wild-type cells, Srv2–GFP was recruited to cortical patches several seconds after the initial assembly of the actin patch (Fig. 5H,I, blue arrowheads) and reached its maximum concentration with the same timing as Abp1p (Fig. 5H,I, red arrowheads). Deletion of the CARP domain barely affected the timing of Srv2p recruitment (Fig. 5I, blue arrowheads), suggesting that the CARP domain is unnecessary for Srv2p recruitment. Interestingly, Srv2p that lacked the HFD domain was recruited with almost the same timing as Abp1p, whereas deletion of the PWP region significantly delayed the recruitment of Srv2p to cortical patches (Fig. 5I, blue arrowheads). The fluorescence intensity of Srv2ΔHFD–GFP and Srv2ΔCARP–GFP peaked at almost the same time point as Abp1–mCherry, whereas Srv2ΔPWP–GFP showed a marked delay (Fig. 5I, red arrowheads).

Functional dissection of the PWP domain in Srv2p localization and actin assembly at the cortical patches

We next verified the phenotypes of the domain-deletion mutants, by comparing them to the phenotypes of several point mutants

Journal of Cell Science (2016) 129, 367-379 doi:10.1242/jcs.176651

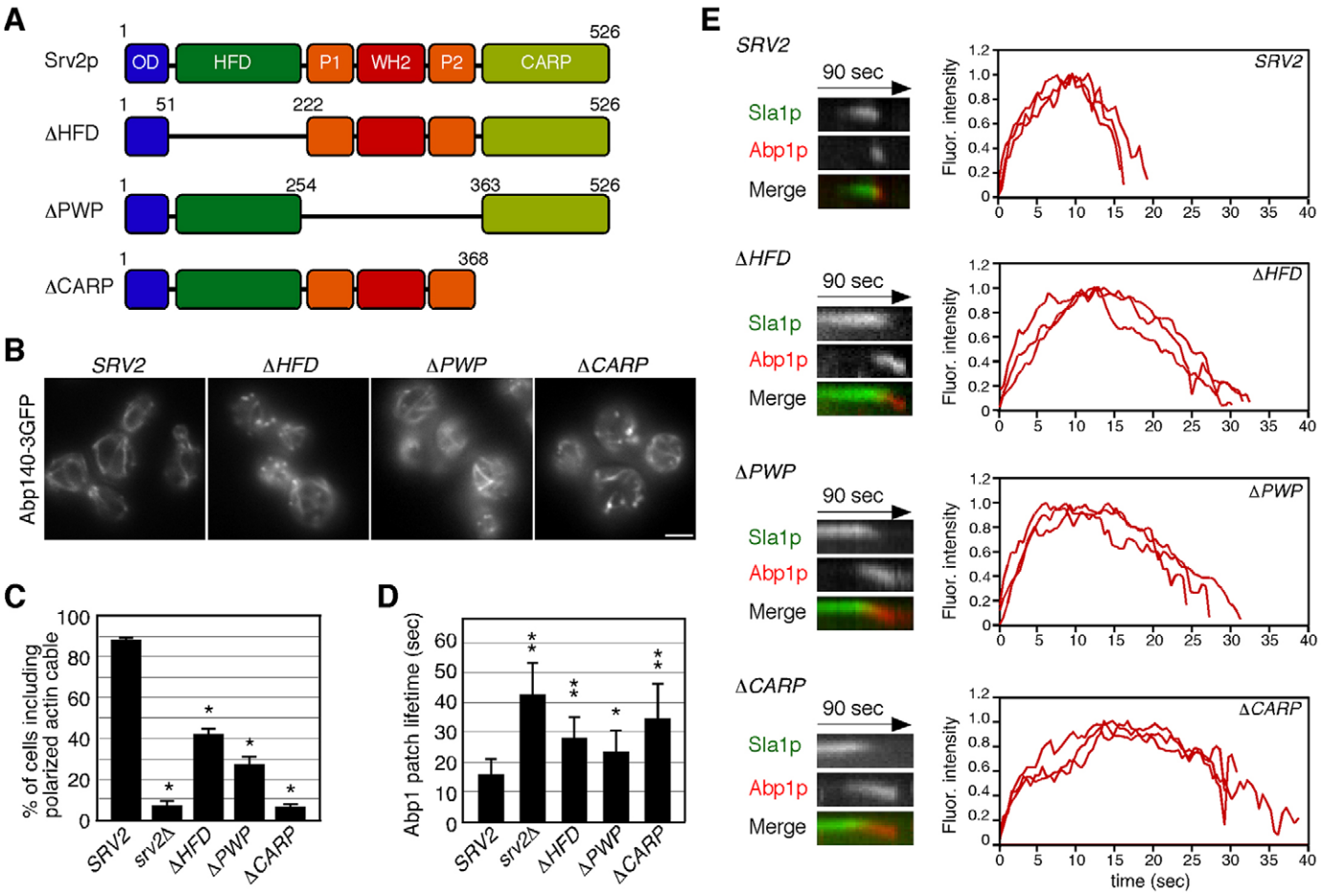

Fig. 4. The effects of domain deletions of Srv2p on actin patch and cable formation. (A) Diagram of wild-type Srv2p and the domain-deletion mutants used in this study. N-terminal oligomerization domain (OD), HFD domain, two proline-rich motifs (P1 and P2), Wasp homology 2 (WH2) domain and C-terminal CARP domains are indicated. (B) The localization of actin cables and patches in Srv2p domain-deletion mutants. Scale bar: 2.5 µm. (C) The bar graphs represent the percentage of wild-type and *srv2*Δ cells that contained polarized actin cables (*n*=100 cells for each strain). **P*<0.001, unpaired Student's *t*-test. Data are means±s.d. (D) Average lifetimes of Abp1–mCherry±s.d. in Srv2p domain-deletion mutants. Data were taken from a 2-min movie with a 1-s frame interval. *n*=50 patches for each strain. **P*<0.001, ***P*<0.001, unpaired Student's *t*-test. (E) Dynamics of the actin patch in Srv2p domain-deletion mutants. Kymograph representations of Sla1–GFP and Abp1–mCherry from 90-s movies are shown in the left-hand panels. The right-hand graphs show the changes in fluorescence intensity of forming patches as a function of time for Abp1–mCherry patches in indicated strains. Each curve represents data from one patch. The behavior of three independent patches was plotted for each strain.

(Fig. 6A) that have been previously generated and biochemically characterized (Bertling et al., 2007; Chaudhry et al., 2010; Mattila et al., 2004; Quintero-Monzon et al., 2009). Srv2-91 contains four alanine residue substitutions at conserved solvent-exposed residues (RILKE mutated to AIAAA) in the HFD domain and has defects in binding to the cofilin–actin complex, and thus defects in cofilin-mediated actin turnover (Quintero-Monzon et al., 2009). Srv2-104 contains replacements of two charged residues with two alanine residues (ENYE mutated to ANYA) in the CARP domain and shows reduced affinity for ADP-actin *in vitro* (Mattila et al., 2004). Each mutant was integrated into the endogenous *SRV2* locus, replacing the original gene. These point mutants displayed no apparent defects in growth at 37°C (Fig. 6B). Similar to the *srv2ΔHFD* mutant (Figs 4D and 5C), the *srv2-91* mutant showed increased lifetimes of Abp1p and Srv2p (~30±11, and 28±12 s; mean±s.d.) (Fig. 6C). GFP-fused Srv2-91 also exhibited a higher fluorescence intensity and was also recruited to cortical patches with almost the same timing as Abp1p (Fig. 6D,F,G), indicating that the phenotypes in these assays caused by deletion of the HFD domain (Fig. 5F,I) are the result of defective binding to the cofilin–actin complex. The *srv2-104* mutant also showed similar defects to the *srv2ΔCARP* mutant (compare Fig. 6C,G to Figs 4D and 5C,I), suggesting that the phenotypes observed in the *srv2ΔCARP* mutant are caused by defective binding to actin monomers.

srv2-201, *srv2-98* and *srv2-203* contain mutations in the P1 (PPP mutated to AAA), WH2 (LKKV mutated to AAAA) and P2 regions (PPP mutated to AAA), respectively (Fig. 6A), and show major defects in binding to profilin, ATP- and ADP-actin, and Abp1p, respectively (Bertling et al., 2007; Chaudhry et al., 2010). Among these, the *srv2-98* mutant exhibited increased lifetimes of Abp1p and Srv2p (~29±11 and 25±10 s, respectively), whereas *srv2-201* and *srv2-203* mutants had no obvious defect in the lifetime of Abp1p, compared to that in wild-type cells (Fig. 6C). In contrast, the *srv2-203* mutant exhibited significantly decreased Srv2p localization at cortical patches, whereas *srv2-201* and *srv2-98* exhibited only modest effects on the localization (Fig. 6E,F). Additionally, similar to Srv2ΔPWP, the timing of Srv2p recruitment to actin patches was markedly delayed in the *srv2-203* mutant (Fig. 6G). These results suggest that the defective localization of Srv2p observed in the *srv2ΔPWP* mutant is caused by defective binding to Abp1p through the P2 region.

Journal of Cell Science (2016) 129, 367-379 doi:10.1242/jcs.176651

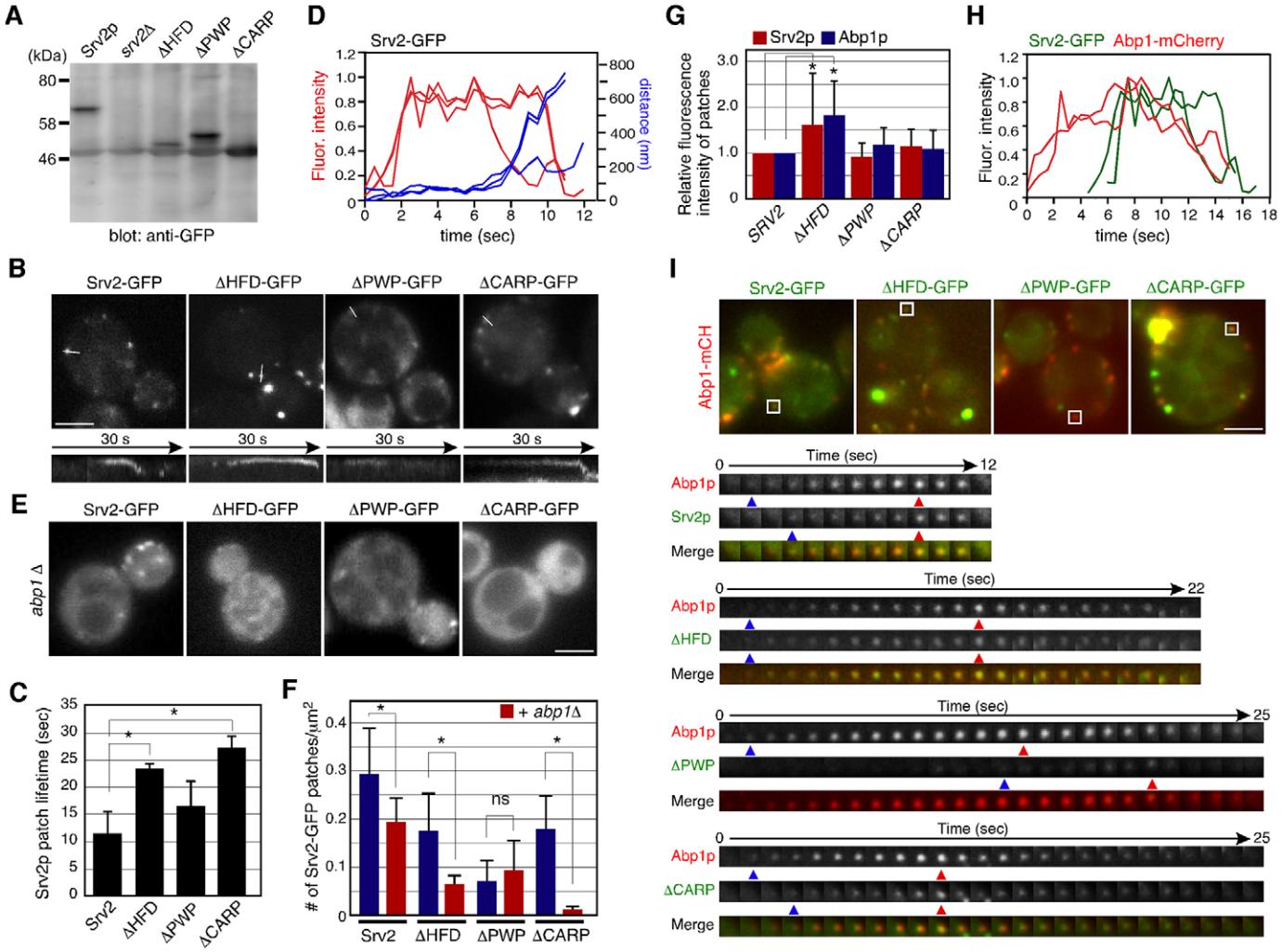

Fig. 5. Localization and dynamics of Srv2p and its domain-deletion mutants. (A) Immunoblots showing the expression of GFP-fused Srv2p and its domain-deletion mutants. 10 µg of whole-cell extracts from each strain were loaded per lane and immunoblotted with an antibody against GFP. (B) The localization of GFP-fused Srv2p and its domain-deletion mutants. Lines in the image mark where the kymograph was generated. Kymograph representations of Srv2–GFP from 30-s movies are shown in the bottom panels. (C) Average lifetimes of Srv2–GFP patches±s.d. in wild-type and mutant cells. Data were taken from 1-min movies with a 1-s frame interval. n>50 patches for each strain. *P<0.001, unpaired t-test. (D) Quantification of fluorescence intensity (fluor.; red) and distance from the site of patch formation (blue) as a function of time for patches of Srv2–GFP. Each curve represents data from one patch. The behavior of three independent patches was plotted for each strain. (E) The localization of GFP-fused Srv2p and its domain-deletion mutants in *abp1*Δ cells. (F) Quantification of the number of Srv2p patches in wild-type and domain-mutant cells. Maximum intensity projections of z-stacks of wild-type and mutant cells labeled with Srv2–GFP were used for calculating the number. The z-stack images were acquired through the entire cell at 0.2-µm intervals. n>30 cells for each strain. *P<0.001, unpaired Student's t-test. ns, not statistically significant. (G) Relative fluorescence intensities of Srv2–GFP and Abp1–mCherry at cortical patches in the indicated strains. Quantification of relative fluorescence intensity of cortical patches, as described in the Materials and Methods. *P<0.001, unpaired Student's t-test. (H) Quantification of the fluorescence intensity of forming patches as a function of time for patches of Srv2–GFP and Abp1–mCherry. Each curve represents data from one patch. The behavior of two independent patches was plotted. (I) Single frames from movies of wild-type and mutant cells showing merged images of the GFP (Srv2p) and the mCherry (Abp1p) channel. Each image pair was acquired simultaneously using dual-channel time-lapse imaging system. A time series of single patches in the boxed area for each strain are shown in the lower panels. Blue arrowheads indicate the appearance of patch fluorescence, and red arrowheads indicate the peak fluorescence. Scale bars: 2.5 µm.

Srv2p functions together with cofilin to accelerate actin turnover

To further analyze the mechanism of Srv2p recruitment to actin patches, we examined Srv2p localization in *sla2*Δ cells, in which endocytic internalization is defective and actin comet tails are stably assembled from endocytic sites in the cell cortex (Kaksonen et al., 2003). Interestingly, we found that Srv2–GFP exhibited a localization that was distinct from the Abp1–mCherry-labeled actin structures in *sla2*Δ cells (Fig. 7A,B, upper panels; Movie 7). The localization of Srv2p and Abp1p was quantified as a function of fluorescence intensity along the actin comet tail. As shown in Fig. 7C, the peak of Srv2–GFP intensity was located at the cytoplasmic edges of actin comet tails. Because it has been demonstrated previously that actin subunits actively treadmill through the actin comet tail from the cortex toward the center of the cell (Kaksonen et al., 2003), this observation suggests that Srv2p might bind to and function around the pointed ends of actin filaments, which have abundant ADP-actin. We also examined the effect of each domain-deletion mutant on Srv2p localization in *sla2*Δ cells. A previous study has shown that cells in which both the *SLA2* and *SRV2* genes have been deleted were inviable (Lila and Drubin, 1997). We found that deletion of the CARP domain of Srv2p in the absence of the *SLA2* gene was also

Journal of Cell Science (2016) 129, 367-379 doi:10.1242/jcs.176651

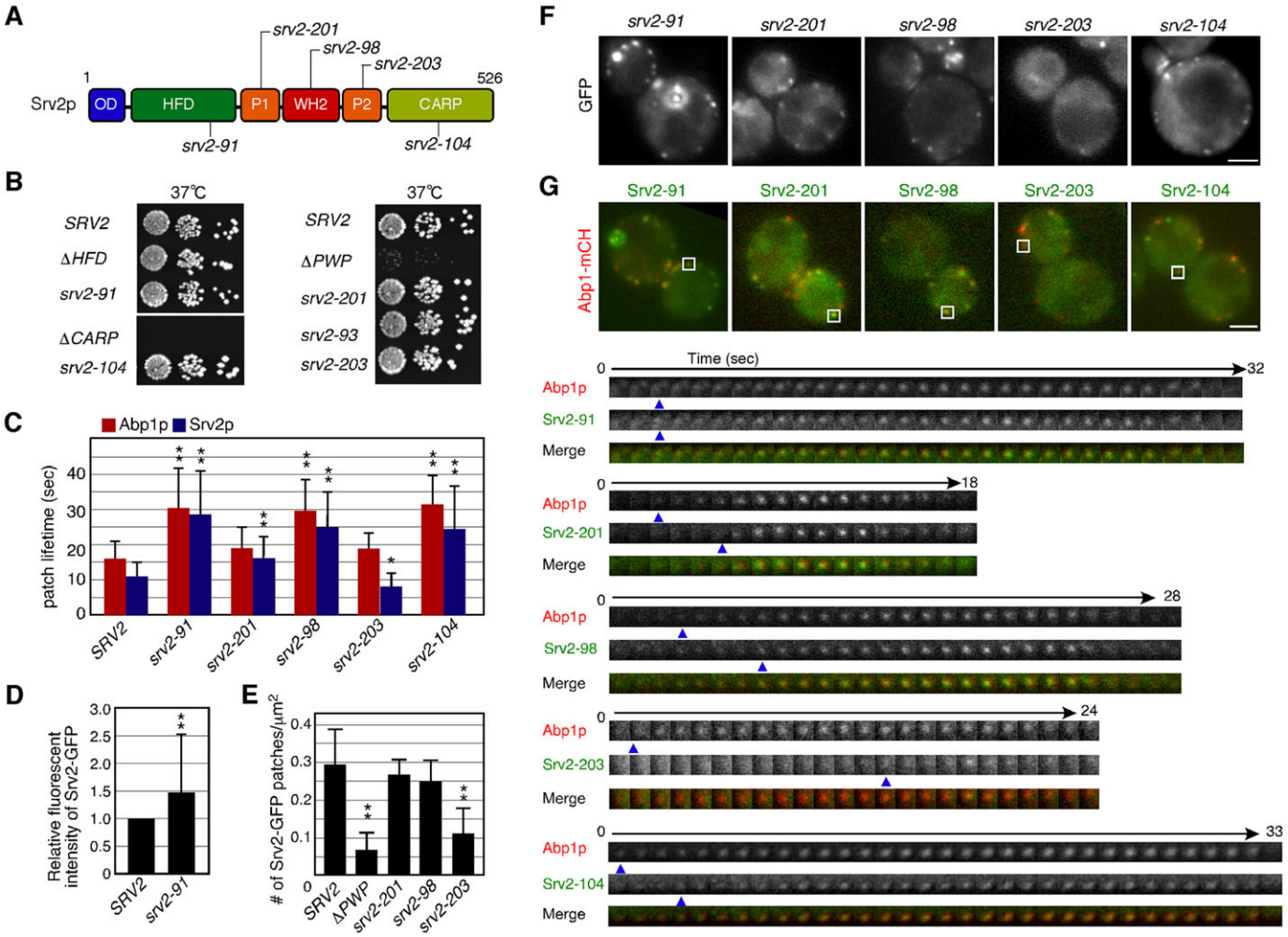

Fig. 6. The effects of point mutations of Srv2p on actin patch formation and Srv2p localization. (A) A diagram of Srv2p indicating the positions of the alanine substitutions found in each mutant. (B) Plates showing the growth phenotype of *SRV2* and *srv2*-mutant strains. Dilution series of the indicated cells were plated onto YPD plates and incubated at 37°C to compare cell growth. (C) Average lifetimes of Abp1–mCherry and Srv2–GFP patches±s.d. in wild-type and mutant cells. Data were taken from 1-min movies with a 1-s frame interval. n>30 patches for each strain. *P<0.01, **P<0.001, unpaired Student's t-test. (D) Relative fluorescence intensities of Srv2–GFP at cortical patches in wild-type and *srv2-91* cells. Quantification was performed as described in the Materials and Methods. n>50 patches for each strain. **P<0.001, unpaired Student's t-test. (E) Quantification of the number of Srv2p patches in wild-type and mutant cells. Maximum intensity projections of z-stacks of wild-type and mutant cells labeled with Srv2–GFP were used to calculate the number. The z-stack images were acquired through the entire cell at 0.2-μm intervals. n>30 cells for each strain. **P<0.001, unpaired Student's t-test. (F) The localization of GFP-fused Srv2p and its point mutants. (G) Single frames from movies of wild-type and mutant cells showing merged images of the GFP (Srv2p) and the mCherry (Abp1p-mCH) channel. Each image pair was acquired simultaneously using a dual-channel time-lapse imaging system. A time series of single patches in the boxed area for each strain are shown in the lower panels. Blue arrowheads indicate the appearance of patch fluorescence. Data are means±s.d. Scale bars: 2.5 μm.

lethal, whereas deletion of the HFD domain or PWP region was non-lethal (Fig. S3B,C). When the PWP region was deleted in *sla2*Δ cells, Srv2ΔPWP–GFP exhibited a localization similar to that of full-length Srv2–GFP, namely at the edges of actin comet tails, the lengths of which were slightly increased (Fig. 7A–C, middle panels and graph; Movie 7). In contrast, deletion of the HFD domain dramatically changed the localization of Srv2p so that it became associated with the actin structures that were labeled entirely with Abp1–mCherry (Fig. 7A–C, lower panels and graph; Movie 7). This observation is consistent with the reported interactions of the HFD domain with F-actin (Jansen et al., 2014). These results suggest that localization of Srv2p to cortical patches through the HFD domain might depend on the nucleotide-bound state of actin, or a protein that has a preferential affinity for ADP-actin.

Srv2p localization at the edges of actin comet tails in *sla2*Δ cells is quite similar to that of Cof1p, yeast cofilin (Okreglak and Drubin, 2007), which exhibits ADP-actin-dependent localization to cortical patches, prompting us to examine the effect of Srv2p domain deletions on Cof1p localization. As expected, Cof1–GFP colocalized with Srv2–mCherry at cortical patches in wild-type cells (Fig. 7D). We also found that Cof1p localized to cortical patches in *srv2*Δ cells as well as in wild-type cells (Fig. 7E), indicating that Cof1p can be recruited to cortical patches independently of Srv2p. Consistent with this idea, deletion of the HFD domain of Srv2p did not affect the localization of Cof1p at the cortical patches (Fig. 7E). Simultaneous two-color imaging revealed that Cof1p is recruited to cortical patches in a manner similar to Srv2p after actin patch assembly in wild-type cells (Fig. 7F). In *srv2*Δ cells, Cof1p was also recruited to cortical patches after actin patch assembly, although its appearance there was substantially delayed (Fig. 7F). Interestingly, in *srv2ΔHFD* cells, Cof1p and Srv2p were recruited to cortical patches with distinct

Journal of Cell Science (2016) 129, 367-379 doi:10.1242/jcs.176651

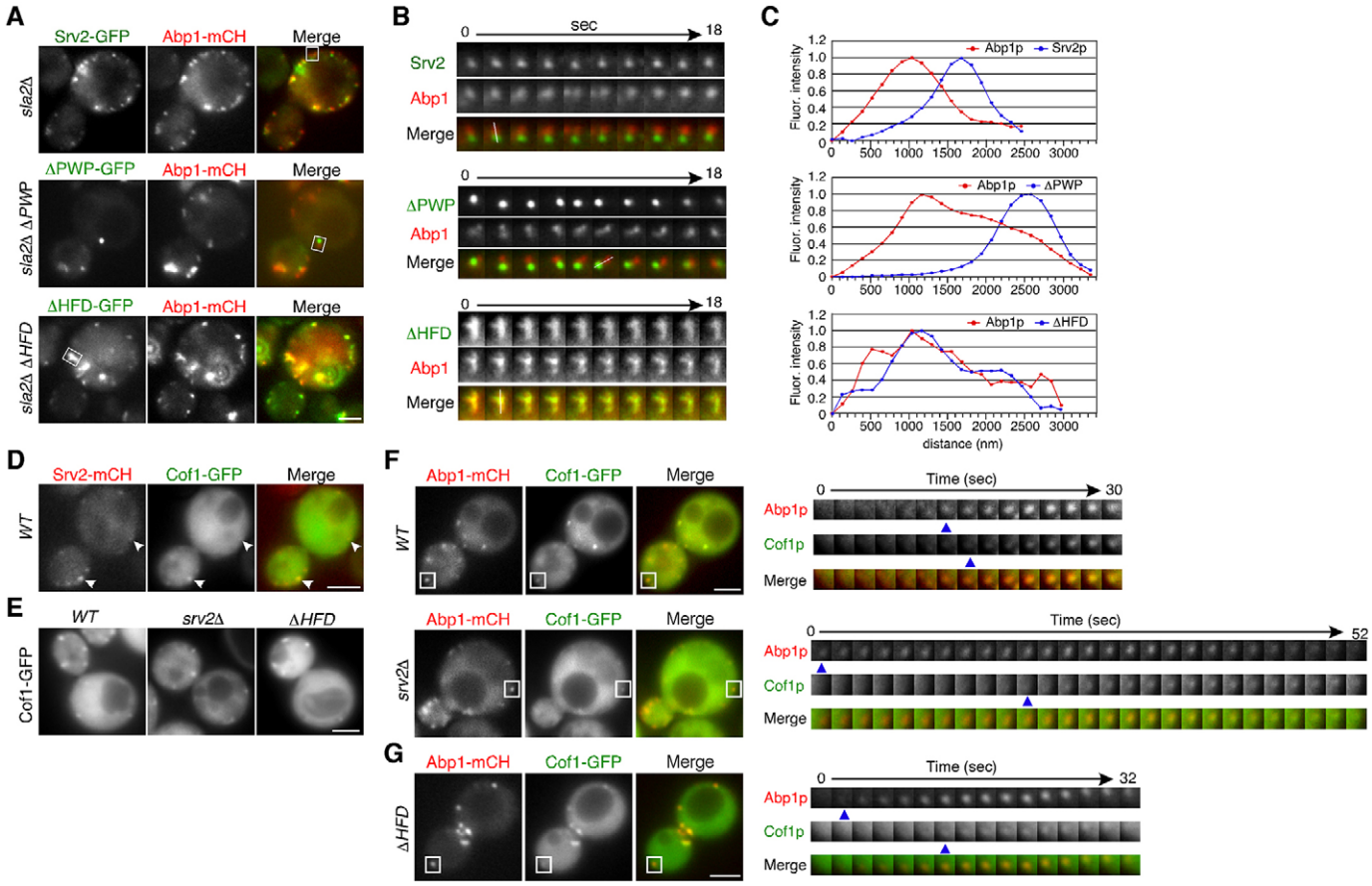

Fig. 7. Dynamic localization of Srv2p and its domain mutants to actin structures in *sla2Δ* cells. (A,B) The localization of full-length Srv2–GFP, Δ*PWP*–GFP and Δ*HFD*–GFP in *sla2*Δ cells expressing Abp1p was captured using simultaneous two-color imaging. (A) Single frames from movies of the indicated genotypes showing the GFP and mCherry (mCH) channels, alongside a merged image. (B) A time series of single patches in the boxed areas shown in A. Lines in the image mark places where fluorescence intensities were analyzed in C. (C) Quantification of the normalized fluorescence intensities of Srv2–GFP and Abp1–mCherry along the length of the actin comet tail in *sla2*Δ cells. The time to acquire one image pair was 2 s. (D) Localization of Cof1–GFP and Srv2–mCherry in wild-type (WT) cells. Each image pair was acquired simultaneously using a dual-channel time-lapse imaging system. (E) The localization of GFP-fused Cof1p in wild type and cells carrying mutations in Srv2p. (F,G) Localization of Cof1–GFP and Abp1–mCherry in wild-type, *srv2*Δ (F) and *srv2*Δ*HFD* (G) cells. Left panels are single frames from movies of the indicated cells showing the GFP (Cof1p) and the mCherry (Srv2p) channels, and a merged image. Each image pair was acquired simultaneously using a dual-channel time-lapse imaging system. Right panels are a time series of single patches in the boxed area in the left panels. The time to acquire one image pair was 2 s. Blue arrowheads indicate the appearance of patch fluorescence. Scale bars: 2.5 µm.

timings – Cof1p was recruited after Abp1p with a little delay (Fig. 7G), whereas Srv2p was recruited simultaneously with Abp1p (Fig. 5I). This observation suggests that localization of Srv2p is not dependent on Cof1p in *srv2*Δ*HFD* cells.

DISCUSSION

Although the function of Srv2p in actin turnover and the physiological importance of Srv2p in maintaining proper actin organization has been established by several previous studies (Balcer et al., 2003; Chaudhry et al., 2013, 2010; Dodatko et al., 2004; Johnston et al., 2015; Ksiazek et al., 2003; Mattila et al., 2004; Quintero-Monzon et al., 2009), the physiological role of Srv2p in endocytic internalization has remained ill defined. We investigated the phenotypes of several *srv2* mutants in living yeast cells and obtained *in vivo* evidence for a requirement of Srv2p in actin cable assembly and endocytic internalization. On the basis of the data presented above and in previous studies, we propose a mechanism of actin patch and cable assembly that is regulated by Srv2p (Fig. 8). In wild-type cells, Srv2p is recruited to cortical patches, through an association with Abp1p (Freeman et al., 1996; Lila and Drubin, 1997; Yu et al., 1999) and Cof1p through the PWP and HFD domains, respectively. The C-terminal CARP domain of Srv2p has a role in recycling ADP-actin to ATP-actin (Balcer et al., 2003; Balderhaar et al., 2013; Chaudhry et al., 2010; Mattila et al., 2004; Moriyama and Yahara, 2002) and, thereby, accelerates the assembly of both actin patches and cables. By contrast, the N-terminal HFD domain catalyzes cofilin-mediated severing of actin filaments (Chaudhry et al., 2013) and could promote actin patch disassembly. Recent studies have suggested a possible role for Cof1p and Aip1p at actin cables, based on observations that Cof1p localizes to actin cables in *aip1*Δ cells (Rodal et al., 1999), and that Cof1p and Aip1p cooperatively promote rapid cable turnover (Okada et al., 2006). Therefore, Cof1p might recruit Srv2p onto actin cables to promote rapid cable turnover (Fig. 8, wild type) (Chaudhry et al., 2013). In contrast, in *srv2*Δ cells, actin turnover through the CARP domain and activation of cofilin by the HFD domain are impaired, and these cause a delay in both the assembly and disassembly of actin patches. The decrease in ATP-actin levels also leads to defective formation of actin cables.

Here, we have demonstrated that deletion of the HFD and PWP domains primarily affects disassembly of actin patches, whereas the CARP domain is required for both assembly and disassembly

Journal of Cell Science (2016) 129, 367-379 doi:10.1242/jcs.176651

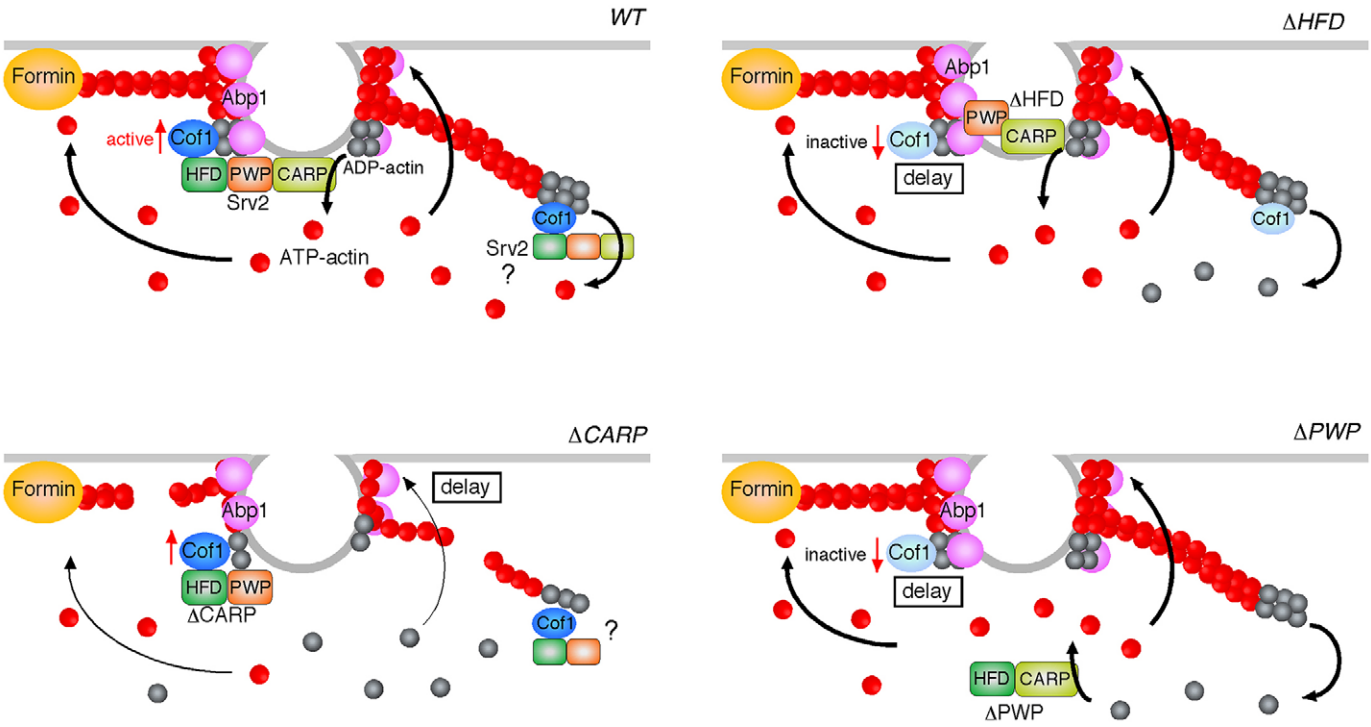

Fig. 8. Model of Srv2p function in regulating actin patch and cable assembly during endocytosis. Srv2p is recruited to cortical patches, dependent on Cof1p and Abp1p, through its HFD and PWP domains. The C-terminal CARP domain of Srv2p has a role in recycling ADP-actin to ATP-actin, and the N-terminal HFD domain catalyzes cofilin-mediated severing of actin filaments. Deletion of the HFD (Δ*HFD*) or PWP (Δ*PWP*) domain changes the localization of Srv2p. In contrast, deletion of the CARP domain (Δ*CARP*) does not change the localization but causes a delay in actin filament turnover. See text for more detailed description. WT, wild type.

of actin patches. Deletion of the HFD domain changed the localization of Srv2p in wild-type and *sla2*Δ cells, and in both cases, Srv2p displayed a different localization from that of Cof1p. The *srv2-91* mutant, which contains a crucial mutation in the HFD, also exhibited phenotypes of altered Srv2p localization and Abp1p dynamics, similar to those seen in the *srv2ΔHFD* mutant. This suggests that Srv2ΔHFD loses the ability to bind to Cof1p, and therefore Cof1p activation by Srv2p is also impaired, causing a delay in actin patch disassembly (Fig. 8, Δ*HFD*). The P2 region of Srv2p functions as a binding site for the SH3 domain of Abp1p during Srv2p localization at cortical actin patches (Freeman et al., 1996; Lila and Drubin, 1997; Yu et al., 1999). We have also demonstrated that deletion of the PWP domain and that the *srv2-203* mutation significantly decreases and/or delays Srv2p recruitment to cortical patches. This causes a delay in Cof1p activation by Srv2p at the cortical patches and results in a delay in actin patch disassembly (Fig. 8, Δ*PWP*). The C-terminal CARP domain of Srv2p is vitally important for the proper assembly of actin patches and cables. In the *srv2ΔCARP* and *srv2-104* mutants, Srv2p is recruited to the cortical patches normally, probably through the HFD and PWP domains, and Cof1p activation is induced normally but is unable to catalyze nucleotide exchange on actin monomers. This probably causes a decreased supply of ATP-actin monomers to be available to the growing end of actin filaments, resulting in a delay in actin patch assembly mediated by the Arp2/3 complex and in actin cable formation mediated by formins (Fig. 8, Δ*CARP*).

Several of our findings in the present study indicate that localization of Srv2p at cortical actin patches is regulated by cofilin as well as Abp1p. First, deletion of the PWP region, even in *abp1*Δ cells, did not completely impair the cortical localization of Srv2p, but deletion of the HFD domain of Srv2p further decreased the cortical localization of Srv2p when expressed in *abp1*Δ cells. As the HFD domain binds directly to F-actin, in addition to its actin-dependent interaction with cofilin (Jansen et al., 2014), the HFD interaction with F-actin also probably contributes to Srv2p localization. Second, Srv2p and Abp1p exhibited apparently different localizations in *sla2*Δ cells, with Abp1p stably associating with the actin comet tail and actively treadmilling through the elongated actin structures (Kaksonen et al., 2003; Okreglak and Drubin, 2007), whereas Srv2p localized only at the cytosolic edges of the actin tail. Interestingly, Cof1p displayed a similar localization to Srv2p in both wild-type and *sla2*Δ cells (Okreglak and Drubin, 2007), suggesting that the *in vivo* localization of Srv2p is dependent on Cof1p, as well as on Abp1p. The reduced binding affinity of Srv2ΔHFD to Cof1p seems to increase the dependency of Srv2p localization on Abp1p. Both Srv2p and cofilin are the most highly conserved proteins that regulate the actin cytoskeleton in eukaryotic cells. There is much evidence for the importance of the interaction between these proteins in actin turnover, both in yeast and mammals (Balcer et al., 2003; Chaudhry et al., 2013; Moriyama and Yahara, 2002; Quintero-Monzon et al., 2009). Additionally, the interaction of Srv2p with cofilin through the HFD domain has also been reported in mammals (Jansen et al., 2014; Moriyama and Yahara, 2002; Quintero-Monzon et al., 2009), suggesting conservation of the mechanisms of Srv2p regulation between yeast and mammals.

*srv2*Δ cells exhibited several unexpected actin cable phenotypes, suggesting that there are, as yet, undiscovered mechanisms regulating the interaction between endocytic vesicles and actin cables. In *srv2*Δ cells, fragmented short actin cables frequently moved toward endocytic sites and moved past them. Actin cables occasionally exhibited a curved structure while moving between two patches in

Journal of Cell Science (2016) 129, 367-379 doi:10.1242/jcs.176651

*srv2*Δ cells, implying that the cables are anchored to endocytic sites and that Srv2 is involved in their proper anchoring. The molecular machinery that attaches actin cables to endocytic sites has not yet been elucidated, although a likely candidate would be an endocytic protein that binds to F-actin. Among such proteins, Sla2p, the yeast homolog of HIP1R, is a potential candidate because it can bind to both the plasma membrane and F-actin through its N-terminal ANTH domain and C-terminal talin-like domain (Sun et al., 2005; Yang et al., 1999). A recent study has shown that Ent1p, the yeast homolog of epsin, is also capable of binding to the membrane and F-actin through its ENTH domain and actin cytoskeleton-binding (ACB) domain (Skruzny et al., 2012). Interestingly, Sla2p and Ent1p can interact redundantly with F-actin, and strains carrying deletions of the actin-binding regions of both proteins exhibit severely defective internalization of endocytic vesicles (Skruzny et al., 2012). The Eps15-like protein Pan1p is another possible candidate because it forms multiple complexes with several endocytic proteins and actin (Goode et al., 2015). Whichever protein is required, our data argues that Srv2p serves to increase its affinity for binding to vesicles or actin cables. Clarifying the mechanism that mediates these interactions is an important area of future study.

MATERIALS AND METHODS

Yeast strains, growth conditions and plasmids

The yeast strains used in this study are listed in Table S1. All strains were grown in standard rich medium (YPD) or synthetic medium supplemented with 2% glucose and appropriate amino acids. C-terminal GFP or mCherry tagging of proteins was performed as described previously (Longtine et al., 1998). Integration plasmids for full-length *SRV2* and for the Δ*HFD*, Δ*PWP* and Δ*CARP SRV2* domain mutants were created as follows: 329 bp of the 5′ UTR, the full length of the *SRV2* open reading frame (nucleotides 1–1581) and 274 bp of the 3′ UTR from the *SRV2* gene were amplified by using PCR and cloned into the *BamH*I site of pBluescript II SK (pBS-*SRV2*). Then, the *Not*I site was destroyed by treating the constructs with the Klenow fragment to create pBS-*SRV2 Not*IΔ. pBS-*SRV2 Not*IΔ was digested by *BstZ171*, and the *Sma*I fragment of the *LEU2* gene was inserted to make pBS-*SRV2 LEU2*. The Δ*HFD*, Δ*PWP* and Δ*CARP* plasmids were generated by ligating the *Not*I-digested PCR products that had been amplified using primers listed in Table S2, using pBS-*SRV2* NotIΔ as a template. To remove the mutations that might have been introduced into the plasmids, the resultant plasmids were digested with *Aor*51HI and *Mlu*I, and the *Aor51*HI-*Mlu*I-digested fragment (containing the Δ*HFD*, Δ*PWP* or Δ*CARP* fragments) was inserted into the *Aor*51HI- and *Mlu*I-digested pBS-*SRV2 LEU2* construct to replace the full-length *SRV2* gene with each mutant. Specific point mutations were introduced through site-directed mutagenesis using the pairs of mutagenic oligonucleotides listed in Table S2. To integrate *srv2* mutants at the endogenous locus of the *SRV2* gene, the plasmids were digested with *BamH*I and transformed into *srv2*Δ cells.

Fluorescence microscopy

Fluorescence microscopy was performed using an Olympus IX81 microscope equipped with a ×100/NA 1.40 (Olympus) objective and an Orca-AG cooled CCD camera (Hamamatsu), using Metamorph software (Universal Imaging). Simultaneous imaging of red and green fluorescence was performed using an Olympus IX81 microscope, described above, and an image splitter (Dual-View; Optical Insights) that divided the red and green components of the images with a 565-nm dichroic mirror and that passed the red component through a 630/50 nm filter and the green component through a 530/30 nm filter. FM4-64 staining was performed as described previously (Toshima et al., 2005).

Fluorescence labeling of α-factor and endocytosis assays

Fluorescence labeling of α-factor was performed as described previously (Toshima et al., 2006). For endocytosis assays, cells were grown to an OD_{600} of ∼0.5 in 0.5 ml YPD, briefly centrifuged, and resuspended in 20 µl of synthetic medium with 5 µM of Alexa-Fluor-594-labeled α-factor. After incubation on ice for 2 h, the cells were washed with ice-cold synthetic medium. Internalization was initiated by addition of synthetic medium that contained 4% glucose and amino acids at 25°C.

^{35}S-labeled α-factor internalization and binding assay

Preparation and internalization of ^{35}S-labeled α-factor was performed as described previously (Toshima et al., 2005). For the binding assay, cells were grown to an OD_{600} of ∼0.3 in 1 ml YPD at 25°C, briefly centrifuged, and resuspended in 50 µl of synthetic medium with 1% (w/v) bovine serum albumin (BSA) and ^{35}S-labeled α-factor on ice. After incubation on ice for 2 h, cells were washed with ice-cold synthetic medium, and the radioactivity was then measured.

Western blot assay

Immunoblot analysis was performed as described previously (Toshima et al., 2005). The antibody against GFP (Life Technologies, A-11122) was used at a dilution of 1:500, and the rabbit anti-mouse IgG conjugated to horseradish peroxidase (Amersham Biosciences, Piscataway, NJ) at 1:1000 dilution was used as the secondary antibody. Immunoreactive protein bands were visualized using ELC plus (GE Healthcare).

Image analysis

The fluorescence intensity of cortical patches in wild-type cells was calculated by averaging the fluorescence intensities of the center area (1×1 pixel area) of individual patches. To calculate the relative fluorescence intensity in mutants, the average fluorescence intensity of the center area of the patch in mutant cells was divided by the average fluorescence intensity of this area in wild-type cells. The fluorescence intensity of actin cables in wild-type cells was calculated by averaging the fluorescence intensities of a randomly selected area (1×1 pixel area) from at least 20 actin cables. For the relative fluorescence intensity of actin cables in mutants, the fluorescence intensity of a randomly selected area (1×1 pixel area) in 50 actin cables was divided by the average fluorescence intensity of actin cables in wild-type cells. The fluorescence intensity was analyzed by using the program ImageJ v1.44.

Acknowledgements

We are grateful to Anthony Bretscher (Cornell University, NY) for providing the *bni1-12 bnr1*Δ (Y4135) strain.

Competing interests

The authors declare no competing or financial interests.

Author contributions

J.Y.T., C.H., A.O., M.N.H., M.N., A.M. and W.Y. performed the experiments and analyzed the data. J.Y.T and J.T. designed and conducted experiments. J.Y.T., D.E.S. and J.T. interpreted the results and wrote the paper.

Funding

J.Y.T. was supported by a Japan Society for the Promotion of Science (JSPS) KAKENHI grant [grant number 26440067]; the Takeda Science Foundation; and the Novartis Foundation (Japan). J.T. was supported by a JSPS KAKENHI grant [grant number 25440054]; the Takeda Science Foundation; and the Kurata Memorial Hitachi Science and Technology Foundation. D.E.S. was supported by the European Union [grant number PCIG12-GA-2012-334077].

Supplementary information

Supplementary information available online at
http://jcs.biologists.org/lookup/suppl/doi:10.1242/jcs.176651/-/DC1

References

Adams, A. E. M., Botstein, D. and Drubin, D. G. (1991). Requirement of yeast fimbrin for actin organization and morphogenesis in vivo. *Nature* **354**, 404-408.

Amatruda, J. F. and Cooper, J. A. (1992). Purification, characterization, and immunofluorescence localization of Saccharomyces cerevisiae capping protein. *J. Cell Biol.* **117**, 1067-1076.

Amberg, D. C. (1998). Three-dimensional imaging of the yeast actin cytoskeleton through the budding cell cycle. *Mol. Biol. Cell* **9**, 3259-3262.

Balcer, H. I., Goodman, A. L., Rodal, A. A., Smith, E., Kugler, J., Heuser, J. E. and Goode, B. L. (2003). Coordinated regulation of actin filament turnover by a

high-molecular-weight Srv2/CAP complex, cofilin, profilin, and Aip1. *Curr. Biol.* **13**, 2159-2169.
Balderhaar, H. J. K., Lachmann, J., Yavavli, E., Brocker, C., Lurick, A. and Ungermann, C. (2013). The CORVET complex promotes tethering and fusion of Rab5/Vps21-positive membranes. *Proc. Natl. Acad. Sci. USA* **110**, 3823-3828.
Bertling, E., Quintero-Monzon, O., Mattila, P. K., Goode, B. L. and Lappalainen, P. (2007). Mechanism and biological role of profilin-Srv2/CAP interaction. *J. Cell Sci.* **120**, 1225-1234.
Bretscher, A. (2003). Polarized growth and organelle segregation in yeast: the tracks, motors, and receptors. *J. Cell Biol.* **160**, 811-816.
Chaudhry, F., Little, K., Talarico, L., Quintero-Monzon, O. and Goode, B. L. (2010). A central role for the WH2 domain of Srv2/CAP in recharging actin monomers to drive actin turnover in vitro and in vivo. *Cytoskeleton* **67**, 120-133.
Chaudhry, F., Breitsprecher, D., Little, K., Sharov, G., Sokolova, O. and Goode, B. L. (2013). Srv2/cyclase-associated protein forms hexameric shurikens that directly catalyze actin filament severing by cofilin. *Mol. Biol. Cell* **24**, 31-41.
Dodatko, T., Fedorov, A. A., Grynberg, M., Patskovsky, Y., Rozwarski, D. A., Jaroszewski, L., Aronoff-Spencer, E., Kondraskina, E., Irving, T., Godzik, A. et al. (2004). Crystal structure of the actin binding domain of the cyclase-associated protein. *Biochemistry* **43**, 10628-10641.
Engqvist-Goldstein, A. E. Y. and Drubin, D. G. (2003). Actin assembly and endocytosis: from yeast to mammals. *Annu. Rev. Cell Dev. Biol.* **19**, 287-332.
Evangelista, M., Pruyne, D., Amberg, D. C., Boone, C. and Bretscher, A. (2002). Formins direct Arp2/3-independent actin filament assembly to polarize cell growth in yeast. *Nat. Cell Biol.* **4**, 32-41.
Freeman, N. L., Lila, T., Mintzer, K. A., Chen, Z., Pahk, A. J., Ren, R., Drubin, D. G. and Field, J. (1996). A conserved proline-rich region of the Saccharomyces cerevisiae cyclase-associated protein binds SH3 domains and modulates cytoskeletal localization. *Mol. Cell. Biol.* **16**, 548-556.
Goode, B. L., Eskin, J. A. and Wendland, B. (2015). Actin and endocytosis in budding yeast. *Genetics* **199**, 315-358.
Gurunathan, S., Chapman-Shimshoni, D., Trajkovic, S. and Gerst, J. E. (2000). Yeast exocytic v-SNAREs confer endocytosis. *Mol. Biol. Cell* **11**, 3629-3643.
Huckaba, T. M., Gay, A. C., Pantalena, L. F., Yang, H.-C. and Pon, L. A. (2004). Live cell imaging of the assembly, disassembly, and actin cable-dependent movement of endosomes and actin patches in the budding yeast, Saccharomyces cerevisiae. *J. Cell Biol.* **167**, 519-530.
Jansen, S., Collins, A., Golden, L., Sokolova, O. and Goode, B. L. (2014). Structure and mechanism of mouse cyclase-associated protein (CAP1) in regulating actin dynamics. *J. Biol. Chem.* **289**, 30732-30742.
Jansen, S., Collins, A., Chin, S. M., Ydenberg, C. A., Gelles, J. and Goode, B. L. (2015). Single-molecule imaging of a three-component ordered actin disassembly mechanism. *Nat. Commun.* **6**, 7202.
Johnston, A. B., Collins, A. and Goode, B. L. (2015). High-speed depolymerization at actin filament ends jointly catalysed by Twinfilin and Srv2/CAP. *Nat. Cell Biol.* **17**, 1504-1511.
Kaksonen, M., Sun, Y. and Drubin, D. G. (2003). A pathway for association of receptors, adaptors, and actin during endocytic internalization. *Cell* **115**, 475-487.
Kaksonen, M., Toret, C. P. and Drubin, D. G. (2005). A modular design for the clathrin- and actin-mediated endocytosis machinery. *Cell* **123**, 305-320.
Kaksonen, M., Toret, C. P. and Drubin, D. G. (2006). Harnessing actin dynamics for clathrin-mediated endocytosis. *Nat. Rev. Mol. Cell Biol.* **7**, 404-414.
Kim, K., Yamashita, A., Wear, M. A., Maeda, Y. and Cooper, J. A. (2004). Capping protein binding to actin in yeast: biochemical mechanism and physiological relevance. *J. Cell Biol.* **164**, 567-580.
Ksiazek, D., Brandstetter, H., Israel, L., Bourenkov, G. P., Katchalova, G., Janssen, K.-P., Bartunik, H. D., Noegel, A. A., Schleicher, M. and Holak, T. A. (2003). Structure of the N-terminal domain of the adenylyl cyclase-associated protein (CAP) from Dictyostelium discoideum. *Structure* **11**, 1171-1178.
Lila, T. and Drubin, D. G. (1997). Evidence for physical and functional interactions among two Saccharomyces cerevisiae SH3 domain proteins, an adenylyl cyclase-associated protein and the actin cytoskeleton. *Mol. Biol. Cell* **8**, 367-385.
Lin, M.-C., Galletta, B. J., Sept, D. and Cooper, J. A. (2010). Overlapping and distinct functions for cofilin, coronin and Aip1 in actin dynamics in vivo. *J. Cell Sci.* **123**, 1329-1342.
Longtine, M. S., McKenzie, A., III, Demarini, D. J., Shah, N. G., Wach, A., Brachat, A., Philippsen, P. and Pringle, J. R. (1998). Additional modules for versatile and economical PCR-based gene deletion and modification in Saccharomyces cerevisiae. *Yeast* **14**, 953-961.
Mattila, P. K., Quintero-Monzon, O., Kugler, J., Moseley, J. B., Almo, S. C., Lappalainen, P. and Goode, B. L. (2004). A high-affinity interaction with ADP-actin monomers underlies the mechanism and in vivo function of Srv2/cyclase-associated protein. *Mol. Biol. Cell* **15**, 5158-5171.
Moriyama, K. and Yahara, I. (2002). Human CAP1 is a key factor in the recycling of cofilin and actin for rapid actin turnover. *J. Cell Sci.* **115**, 1591-1601.
Moseley, J. B. and Goode, B. L. (2006). The yeast actin cytoskeleton: from cellular function to biochemical mechanism. *Microbiol. Mol. Biol. Rev.* **70**, 605-645.
Okada, K., Ravi, H., Smith, E. M. and Goode, B. L. (2006). Aip1 and cofilin promote rapid turnover of yeast actin patches and cables: a coordinated mechanism for severing and capping filaments. *Mol. Biol. Cell* **17**, 2855-2868.
Okreglak, V. and Drubin, D. G. (2007). Cofilin recruitment and function during actin-mediated endocytosis dictated by actin nucleotide state. *J. Cell Biol.* **178**, 1251-1264.
Ono, S. (2013). The role of cyclase-associated protein in regulating actin filament dynamics - more than a monomer-sequestration factor. *J. Cell Sci.* **126**, 3249-3258.
Perrais, D. and Merrifield, C. J. (2005). Dynamics of endocytic vesicle creation. *Dev. Cell* **9**, 581-592.
Quintero-Monzon, O., Jonasson, E. M., Bertling, E., Talarico, L., Chaudhry, F., Sihvo, M., Lappalainen, P. and Goode, B. L. (2009). Reconstitution and dissection of the 600-kDa Srv2/CAP complex: roles for oligomerization and cofilin-actin binding in driving actin turnover. *J. Biol. Chem.* **284**, 10923-10934.
Rodal, A. A., Tetreault, J. W., Lappalainen, P., Drubin, D. G. and Amberg, D. C. (1999). Aip1p interacts with cofilin to disassemble actin filaments. *J. Cell Biol.* **145**, 1251-1264.
Sagot, I., Klee, S. K. and Pellman, D. (2002). Yeast formins regulate cell polarity by controlling the assembly of actin cables. *Nat. Cell Biol.* **4**, 42-50.
Skruzny, M., Brach, T., Ciuffa, R., Rybina, S., Wachsmuth, M. and Kaksonen, M. (2012). Molecular basis for coupling the plasma membrane to the actin cytoskeleton during clathrin-mediated endocytosis. *Proc. Natl. Acad. Sci. USA* **109**, E2533-E2542.
Sun, Y., Kaksonen, M., Madden, D. T., Schekman, R. and Drubin, D. G. (2005). Interaction of Sla2p's ANTH domain with PtdIns(4,5)P2 is important for actin-dependent endocytic internalization. *Mol. Biol. Cell* **16**, 717-730.
Toshima, J., Toshima, J. Y., Martin, A. C. and Drubin, D. G. (2005). Phosphoregulation of Arp2/3-dependent actin assembly during receptor-mediated endocytosis. *Nat. Cell Biol.* **7**, 246-254.
Toshima, J. Y., Toshima, J., Kaksonen, M., Martin, A. C., King, D. S. and Drubin, D. G. (2006). Spatial dynamics of receptor-mediated endocytic trafficking in budding yeast revealed by using fluorescent alpha-factor derivatives. *Proc. Natl. Acad. Sci. USA* **103**, 5793-5798.
Toshima, J. Y., Nishinoaki, S., Sato, Y., Yamamoto, W., Furukawa, D., Siekhaus, D. E., Sawaguchi, A. and Toshima, J. (2014). Bifurcation of the endocytic pathway into Rab5-dependent and -independent transport to the vacuole. *Nat. Commun.* **5**, 3498.
Wesp, A., Hicke, L., Palecek, J., Lombardi, R., Aust, T., Munn, A. L. and Riezman, H. (1997). End4p/Sla2p interacts with actin-associated proteins for endocytosis in Saccharomyces cerevisiae. *Mol. Biol. Cell* **8**, 2291-2306.
Winter, D., Podtelejnikov, A. V., Mann, M. and Li, R. (1997). The complex containing actin-related proteins Arp2 and Arp3 is required for the motility and integrity of yeast actin patches. *Curr. Biol.* **7**, 519-529.
Yang, H.-C. and Pon, L. A. (2002). Actin cable dynamics in budding yeast. *Proc. Natal. Acad. Sci. USA* **99**, 751-756.
Yang, S., Cope, M. J. T. V. and Drubin, D. G. (1999). Sla2p is associated with the yeast cortical actin cytoskeleton via redundant localization signals. *Mol. Biol. Cell* **10**, 2265-2283.
Yu, J., Wang, C., Palmieri, S. J., Haarer, B. K. and Field, J. (1999). A cytoskeletal localizing domain in the cyclase-associated protein, CAP/Srv2p, regulates access to a distant SH3-binding site. *J. Biol. Chem.* **274**, 19985-19991.

Journal of Cell Science

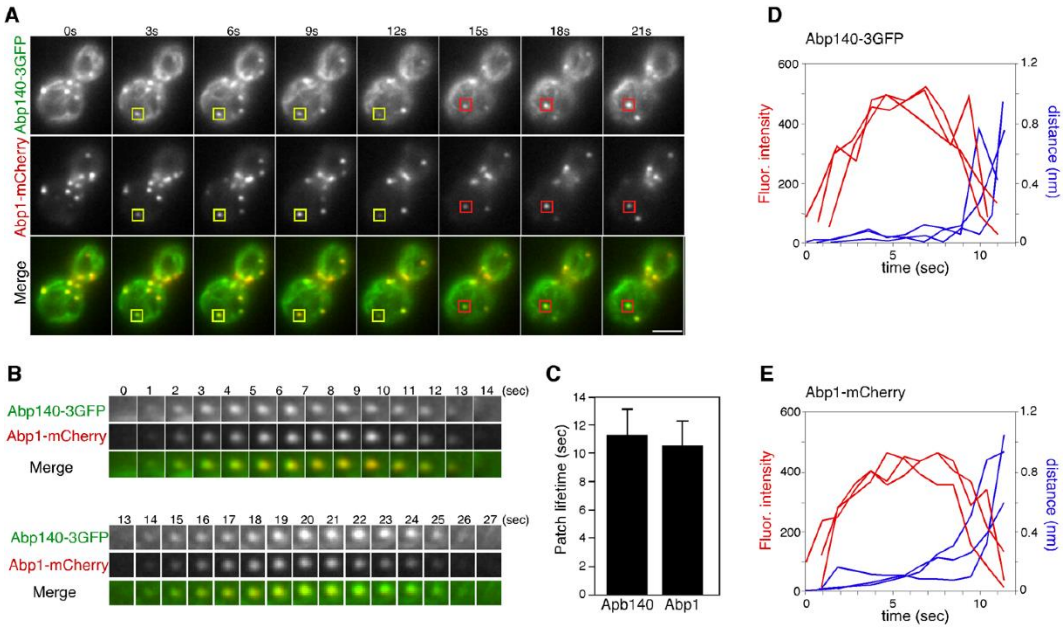

Figure S1. Comparison of the dynamics of Abp1p patches and Abp140 patches. (A) Localization of 3GFP-tagged Abp140p and mCherry-tagged Abp1p in living cells. Each image pair was simultaneously acquired at successive 3 sec intervals using a dual-channel imaging system. Scale bar, 2.5 μm. (B) Higher magnification view of the boxed area in (A). Time series of a single patch and cable from wild-type cells expressing Abp1-RFP and Abp140-3GFP. Time to acquire one image pair was 1 sec. (C) Average lifetimes of Abp140-3GFP- or Abp1-mCherry-labeled patches in wild-type cells. Data were taken from 1-min movies with a 1-sec frame interval. n > 50 patches for each strain. (D, E) Quantification of fluorescence intensity (blue) and distance from the site of patch formation (red) as a function of time for patches of Abp140-3GFP (D) or Abp1-mCherry (E). Each curve represents data from one patch. Behavior of three independent patches was plotted for each strain.

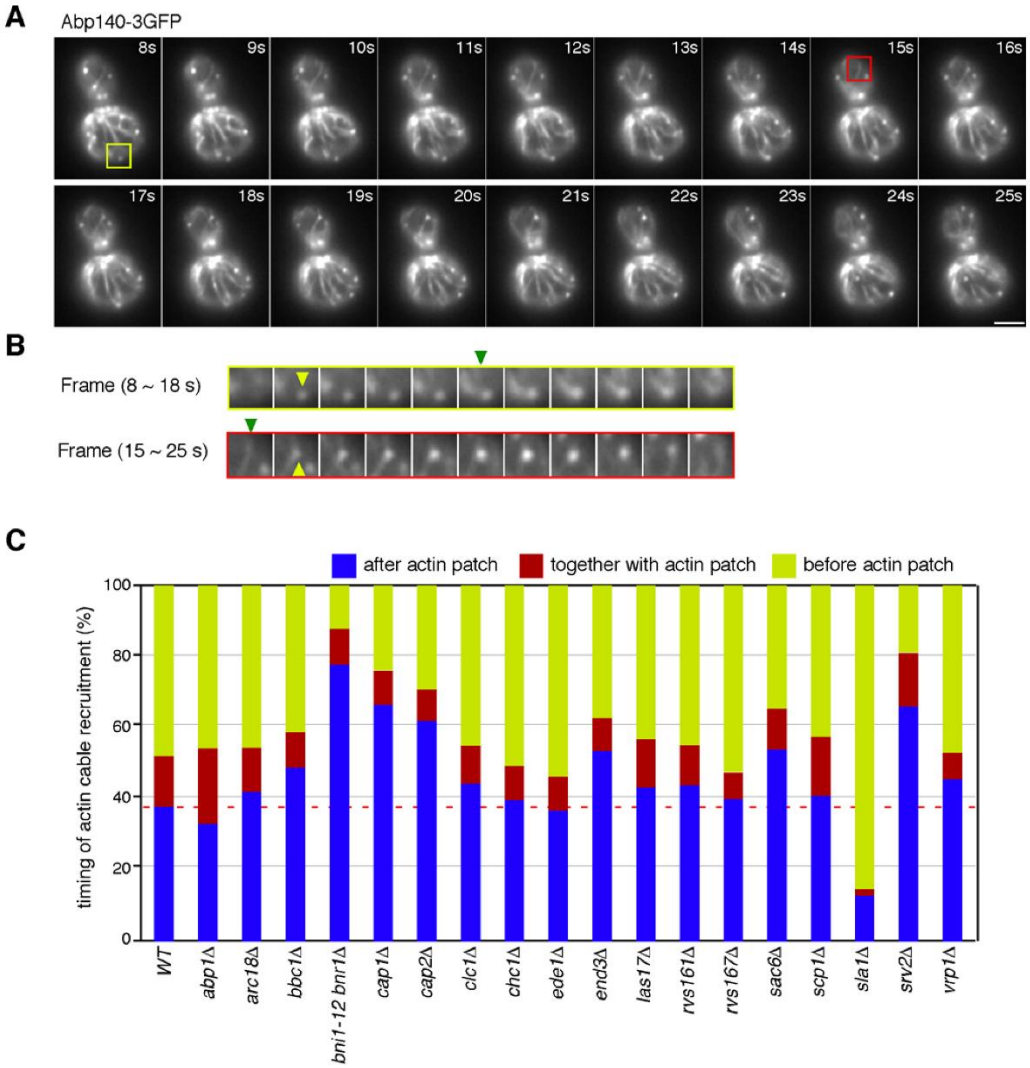

Figure S2. Spatio-temporal recruitment of actin cables to endocytic sites. (A) The dynamics of Abp140-3GFP visualized at the surface of a wild-type cell. Time to acquire one image pair was 1 sec. Arrowheads indicate examples of an actin patch that appears before actin cable recruitment (yellow), or an actin patch that appears after actin cable recruitment (red). Scale bar, 2.5 μm. (B) Higher-magnification view of the boxed areas in (A). Upper panels (8-18 sec) or lower panels (15-25 sec) correspond to the area boxed in Yellow or Red in (A), respectively. Yellow arrowheads in (B) indicate the timing of actin patch appearance and green arrowheads indicate the timing of actin cable recruitment. (C) Quantitative analysis categorizing actin cable recruitment as before (yellow), after (blue), or at the same time as (red) actin patch formation. Data show the mean of two independent experiments, with >30 patches counted for each strain per experiment.

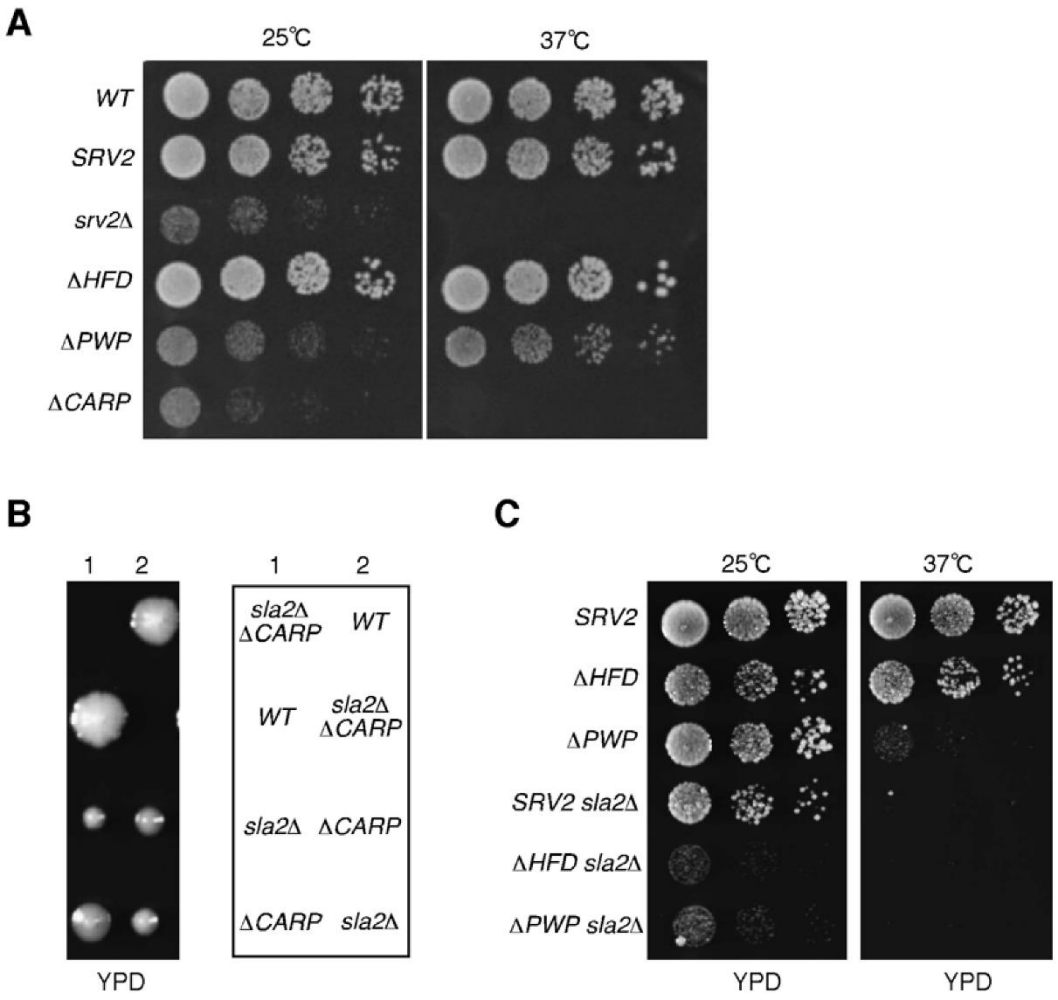

Figure S3. Growth phenotype of Srv2p domain deletion mutants and the genetic interaction between the *srv2* and *sla2* mutants. (A) Plates showing the growth phenotype of Srv2p domain deletion mutants. A dilution series of the indicated cells were plated on YPD plates and incubated at 25°C or 37°C, respectively. (B) Synthetic lethality between *sla2*Δ and *srv2*Δ*CARP* mutants. Tetrad analysis following sporulation of an *sla2*Δ::kan^r/*SLA2 srv2*Δ*CARP*::*LEU2*/*SRV2* diploid. The tetrads were dissected on a YPD plate, and the plate was photographed after 4 days of growth at 25°C. The right panel represents the genotype of each spore. (C) Plates showing the growth phenotype of *sla2* and *srv2* mutants. A dilution series of the indicated cells was plated on YPD plates and incubated at 25°C or 37°C, respectively.

SUPPLEMENTARY MOVIES

Note: for best viewing, movies should be played in the "loop" mode.

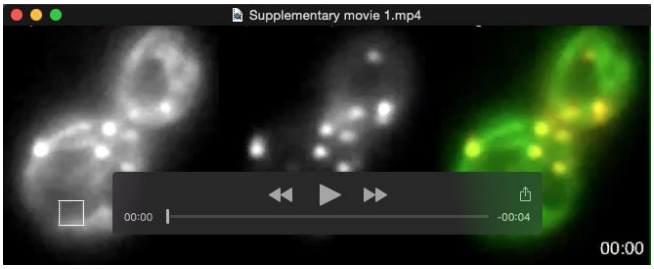

Supplementary movie 1

Localization of Aplp140-3GFP (left; green in merge) and Abp1-mCherry (center; red in merge) in wild-type cells. Within the boxes, examples of colocalization were indicated. Interval between frames is 1 sec**.**

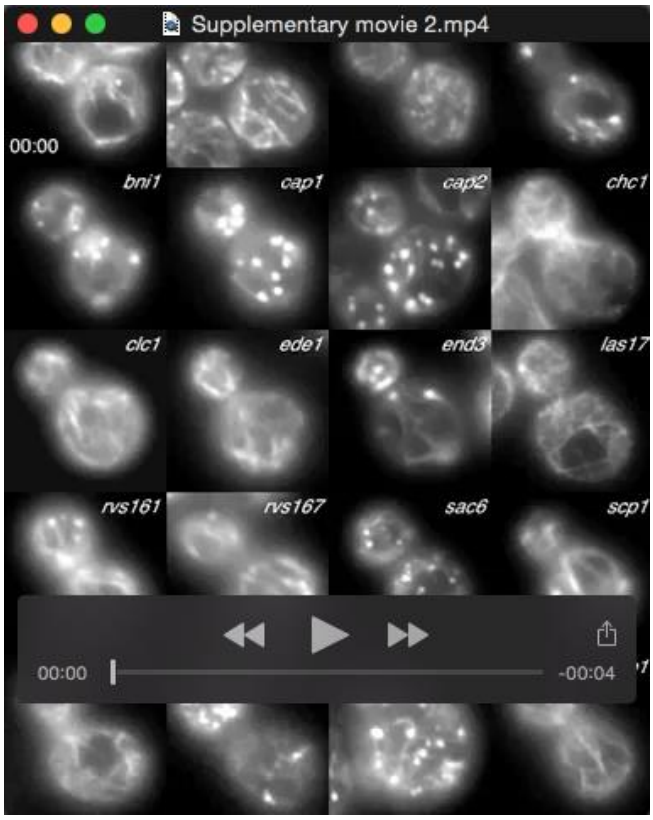

Supplementary movie 2

Localization of Abp140-3GFP in indicated mutant cells. Interval between frames is 1 sec.

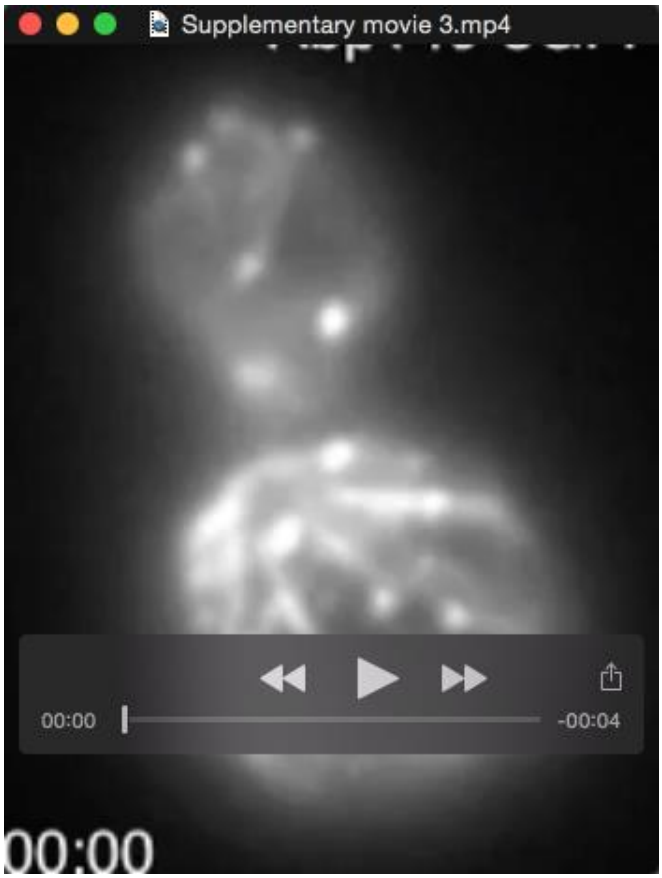

Supplementary movie 3

Localization of Abp140-3GFP in wild-type cells. Interval between frames is 1 sec**.**

Supplementary movie 4

Localization of Abp140-3GFP in *srv2*Δ cell. Arrowheads indicate example of actin cables moving past actin patches. Interval between frames is 1 sec**.**

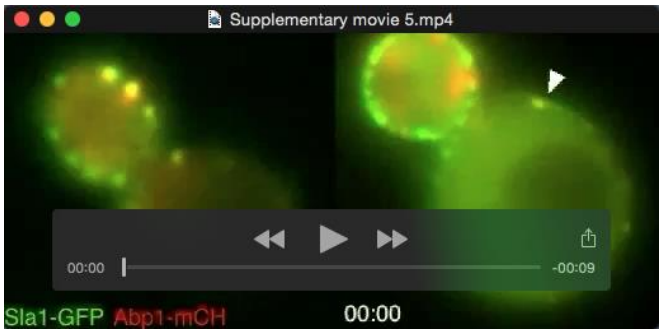

Supplementary movie 5

Localization of Sla1-GFP and Abp1-mCherry in wild-type (left) and *srv2*Δ cells. Arrowheads indicate example of recruitment of Sla1p and Abp1p. Interval between frames is 2 sec**.**

Supplementary movie 6

Localization of GFP-tagged Srv2p and its deletion mutants, and Abp1-mCherry. Arrowheads indicate example of recruitment of Srv2p and Abp1p. Interval between frames is 1 sec**.**

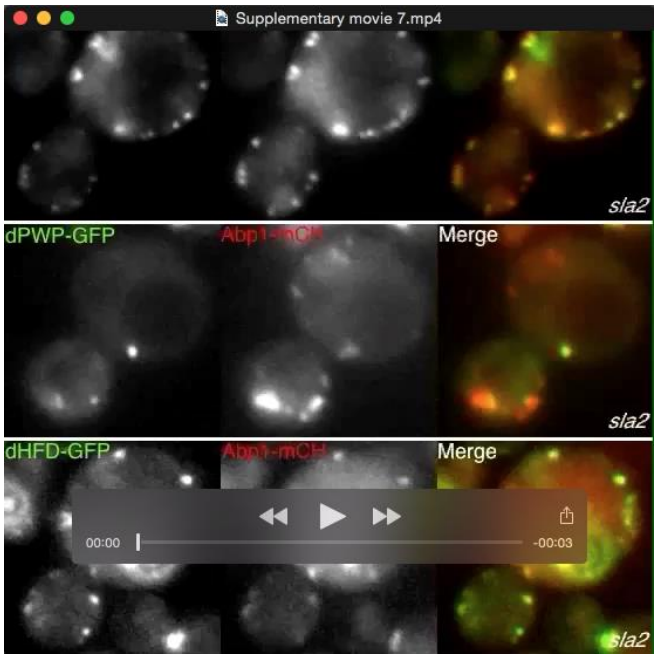

Supplementary movie 7

Localization of GFP-tagged Srv2p and its deletion mutants, and Abp1-mCherry in *sla2*Δ cells. Interval between frames is 1 sec**.**

Supplementary Table 1. Yeast strains

Strain	Genotype	Source
DDY2783	*Mat***a** *his3-Δ200 leu2-3, 112 ura3-52 bar1Δ::LEU2*	
DDY3039	*Mat***a** *his3-Δ200 leu2-3, 112 ura3-52 bar1Δ::LEU2 ABP140-3GFP::HIS3*	
DDY3040	*Matα his3-Δ200 leu2-3, 112 ura3-52 bni1-12::URA3 bnr1Δ::KanMX6 ABP140-3GFP::HIS3*	
JJTY0997	*Mat***a** *his3Δ0 leu2Δ0 ura3Δ0 lys2Δ0 sac6Δ::KanMX6 ABP140-3GFP::HIS3*	This study
JJTY0998	*Mata his3Δ0 leu2Δ0 ura3Δ0 lys2Δ0 rvs167Δ::KanMX6 ABP140-3GFP::HIS3*	This study
JJTY0999	*Mat***a** *his3Δ0 leu2Δ0 ura3Δ0 lys2Δ0 rvs161Δ::KanMX6 ABP140-3GFP::HIS3*	This study
JJTY1000	*Mat***a** *his3Δ0 leu2Δ0 ura3Δ0 lys2Δ0 cap1Δ::KanMX6 ABP140-3GFP::HIS3*	This study
JJTY1001	*Mat***a** *his3Δ0 leu2Δ0 ura3Δ0 lys2Δ0 vrp1Δ::KanMX6 ABP140-3GFP::HIS3*	This study
JJTY1002	*Mat***a** *his3Δ0 leu2Δ0 ura3Δ0 lys2Δ0 chc1Δ::KanMX6 ABP140-3GFP::HIS3*	This study
JJTY1003	*Mat***a** *his3Δ0 leu2Δ0 ura3Δ0 lys2Δ0 clc1Δ::KanMX6 ABP140-3GFP::HIS3*	This study
JJTY1004	*Mat***a** *his3Δ0 leu2Δ0 ura3Δ0 lys2Δ0 sla1Δ::KanMX6 ABP140-3GFP::HIS3*	This study
JJTY1005	*Mat***a** *his3Δ0 leu2Δ0 ura3Δ0 lys2Δ0 ede1Δ::KanMX6 ABP140-3GFP::HIS3*	This study
JJTY1006	*Mat***a** *his3Δ0 leu2Δ0 ura3Δ0 lys2Δ0 cap2Δ::KanMX6 ABP140-3GFP::HIS3*	This study
JJTY1007	*Mat***a** *his3Δ0 leu2Δ0 ura3Δ0 lys2Δ0 bbc1Δ::KanMX6 ABP140-3GFP::HIS3*	This study
JJTY1008	*Mat***a** *his3Δ0 leu2Δ0 ura3Δ0 lys2Δ0 end3Δ::KanMX6 ABP140-3GFP::HIS3*	This study
JJTY1009	*Mat***a** *his3Δ0 leu2Δ0 ura3Δ0 lys2Δ0 arc18Δ::KanMX6 ABP140-3GFP::HIS3*	This study
JJTY1010	*Mat***a** *his3Δ0 leu2Δ0 ura3Δ0 lys2Δ0 sla2Δ::KanMX6 ABP140-3GFP::HIS3*	This study
JJTY1011	*Mat***a** *his3Δ0 leu2Δ0 ura3Δ0 lys2Δ0 abp1Δ::KanMX6 ABP140-3GFP::HIS3*	This study
JJTY1141	*Mat***a** *his3Δ0 leu2Δ0 ura3Δ0 lys2Δ0 scp1Δ::KanMX6 ABP140-3GFP:HIS3 ABP1-mCherry::URA*	This study
JJTY1163	*Mat***a** *his3Δ1 leu2Δ0 ura3Δ0 ABP140-3GFP::HIS3 ABP1-mCherry::URA3*	This study
JJTY1166	*Mat***a** *his3-Δ200 leu2-3, 112 ura3-52 ABP1-mCherry::URA3*	This study
JJTY1128	*Mat***a** *his3Δ0 leu2Δ0 ura3Δ0 lys2Δ0 las17Δ::KanMX6 ABP140-3GFP::HIS3 ABP1-mCherry::URA3*	This study
JJTY1379	*Mat***a** *his3Δ1 leu2Δ0 ura3Δ0 lys2Δ0 srv2Δ:: KanMX6 bar1Δ::LEU2*	This study
JJTY1874	*Mat***a** *his3Δ0 leu2Δ0 ura3Δ0 lys2Δ0 srv2Δ::KanMX6 ABP140-3GFP::HIS3*	This study
JJTY1875	*Mat***a** *his3Δ1 leu2Δ0 ura3Δ0 lys2Δ0 srv2Δ::KanMX6 ABP1-mCherry::URA3*	This study

JJTY2216	*Mat**a** his3Δ1 leu2Δ0 ura3Δ0 lys2Δ0 srv2Δ::KanMX6 SLA1-GFP::HIS ABP1-mCherry::URA*	This study
JJTY2922	*Mat**a** his3Δ1 leu2Δ0 ura3Δ0 lys2Δ0 srv2Δ::SRV2::LEU2 SLA1-GFP::HIS ABP1-mCherry::URA*	This study
JJTY2924	*Mat**a** his3Δ1 leu2Δ0 ura3Δ0 lys2Δ0 srv2Δ::srv2ΔPWP::LEU2 SLA1-GFP::HIS ABP1-mCherry::URA*	This study
JJTY2925	*Mat**a** his3Δ1 leu2Δ0 ura3Δ0 lys2Δ0 srv2Δ::srv2ΔPWP::LEU2 ABP140-3GFP::HIS3*	This study
JJTY2926	*Mat**a** his3Δ1 leu2Δ0 ura3Δ0 lys2Δ0 srv2Δ::srv2ΔCARP::LEU2 SLA1-GFP::HIS ABP1-mCherry::URA*	This study
JJTY2927	*Mat**a** his3Δ1 leu2Δ0 ura3Δ0 lys2Δ0 srv2Δ::srv2ΔCARP::LEU2 ABP140-3GFP::HIS3*	This study
JJTY3096	*Mat**a** his3Δ1 leu2Δ0 ura3Δ0 lys2Δ0 srv2Δ:: srv2ΔHFD::LEU2 SLA1-GFP::HIS ABP1-mCherry::URA*	This study
JJTY3097	*Mat**a** his3Δ1 leu2Δ0 ura3Δ0 lys2Δ0 srv2Δ::SRV2::LEU2 ABP140-3GFP::HIS3*	This study
JJTY3098	*Mat**a** his3Δ1 leu2Δ0 ura3Δ0 lys2Δ0 srv2Δ::srv2ΔHFD::LEU2 ABP140-3GFP::HIS3*	This study
JJTY3323	*Mat**a** his3-Δ200 leu2-3, 112 ura3-52 lys2-801 SRV2-GFP::HIS3*	This study
JJTY3324	*Mat**a** his3-Δ200 leu2-3, 112 ura3-52 lys2-801 srv2Δ::srv2ΔHFD::LEU2 srv2ΔHFD-GFP::HIS3*	This study
JJTY3325	*Mat**a** his3-Δ200 leu2-3, 112 ura3-52 lys2-801 srv2Δ::srv2ΔCARP::LEU2 srv2ΔCARP-GFP::HIS3*	This study
JJTY3326	*Mat**a** his3-Δ200 leu2-3, 112 ura3-52 lys2-801 SRV2-GFP::HIS3 ABP1-mCherry::URA3*	This study
JJTY3488	*Matα his3Δ1 leu2Δ0 ura3Δ0 lys2Δ0 met15Δ0 SLA1-GFP::HIS3 ABP1-mCherry::URA3*	This study
JJTY3613	*Mat**a** his3-Δ200 leu2-3, 112 ura3-52 lys2-801 srv2Δ:: srv2ΔHFD::LEU2 srv2ΔHFD-GFP::HIS3 ABP1-mCherry::URA*	This study
JJTY3891	*Mat**a** his3-Δ200 leu2-3, 112 ura3-52 lys2-801 srv2Δ:: srv2ΔPWP::LEU2 srv2ΔPWP-GFP::HIS3*	This study
JJTY4984	*Mat**a** his3-Δ200 leu2-3, 112 ura3-52 lys2-801 srv2Δ:: srv2ΔHFD::LEU2 Srv2ΔHFD-GFP::HIS3 abp1Δ::URA3*	This study
JJTY4985	*Mat**a** his3-Δ200 leu2-3, 112 ura3-52 lys2-801 srv2Δ:: srv2ΔPWP::LEU2 SRV2ΔPWP-GFP::HIS3 abp1Δ::URA3*	This study
JJTY4986	*Mat**a** his3-Δ200 leu2-3, 112 ura3-52 lys2-801 srv2Δ:: srv2ΔCARP::LEU2 Srv2ΔCARP-GFP::HIS3 abp1Δ::URA3*	This study
JJTY5627	*Mat**a** his3-Δ200 leu2-3, 112 ura3-52 ABP1-mCherry::URA3 COF1-GFP::HIS3*	This study
JJTY5628	*Mat**a** his3Δ1 leu2Δ0 ura3Δ0 lys2Δ0 srv2Δ::srv2ΔHFD::LEU2 COF1-GFP::HIS3*	

	ABP1-mCherry::URA	This study
JJTY5631	*Mat***a** *his3Δ1 leu2Δ0 ura3Δ0 lys2Δ0 srv2Δ::KanMX6 COF1-GFP::HIS3*	
	ABP1-mCherry::URA	This study
JJTY5632	*Mat***a** *his3Δ1 leu2Δ0 ura3Δ0 lys2Δ0 srv2Δ::SRV2::LEU2 COF1-GFP::HIS3*	
	SRV2-mCherry::URA	This study
JJTY5641	*Mat***a** *his3Δ1 leu2Δ0 ura3Δ0 lys2Δ0 sla2Δ::KanMX6 SRV2-GFP::HIS3 ABP1-mCherry::URA*	This study
JJTY5642	*Mat***a** *his3Δ1 leu2Δ0 ura3Δ0 lys2Δ0 sla2Δ::KanMX6 srv2ΔHFD-GFP::HIS3*	
	ABP1-mCherry::URA	This study
JJTY5643	*Mat***a** *his3Δ1 leu2Δ0 ura3Δ0 lys2Δ0 sla2Δ::KanMX6 srv2ΔPWP-GFP::HIS3*	
	ABP1-mCherry::URA	This study
JJTY5651	*Mat***a** *his3-Δ200 leu2-3, 112 ura3-52 lys2-801 srv2Δ:: srv2ΔPWP::LEU2 srv2ΔPWP-GFP::HIS3*	
	ABP1-mCherry::URA	This study
JJTY5652	*Mat***a** *his3-Δ200 leu2-3, 112 ura3-52 lys2-801 srv2Δ:: srv2ΔCARP::LEU2 srv2ΔCARP-GFP::HIS3*	
	ABP1-mCherry::URA	This study
JJTY5914	*Mat***a** *his3-Δ200 leu2-3, 112 ura3-52 lys2-801 srv2Δ:: srv2-91::LEU2 srv2-91-GFP::HIS3*	
	ABP1-mCherry::URA	This study
JJTY5915	*Mat***a** *his3-Δ200 leu2-3, 112 ura3-52 lys2-801 srv2Δ:: srv2-201::LEU2 srv2-201-GFP::HIS3*	
	ABP1-mCherry::URA	This study
JJTY5916	*Mat***a** *his3-Δ200 leu2-3, 112 ura3-52 lys2-801 srv2Δ:: srv2-98::LEU2 srv2-98-GFP::HIS3*	
	ABP1-mCherry::URA	This study
JJTY5917	*Mat***a** *his3-Δ200 leu2-3, 112 ura3-52 lys2-801 srv2Δ:: srv2-203::LEU2 srv2-203-GFP::HIS3*	
	ABP1-mCherry::URA	This study
JJTY5918	*Mat***a** *his3-Δ200 leu2-3, 112 ura3-52 lys2-801 srv2Δ:: srv2-104::LEU2 srv2-104-GFP::HIS3*	
	ABP1-mCherry::URA	This study

Supplementary Table 2. Primers used in this study

Primer	Gene	Sequence	Use
JT1201	*SRV2*	GAAGATCTGCGGCCGCGGAAGGCTTGTTATTTTTAGATGCC	deletion of the HFD domain
JT1202	*SRV2*	GAAGATCTGCGGCCGCTGCCTCTTTCGATAATTTGAAAGCC	deletion of the HFD domain
JT1203	*SRV2*	GAAGATCTGCGGCCGCTGCCATCGCGTCAGCAAAATC	deletion of the PWP domain
JT1204	*SRV2*	GAAGATCTGCGGCCGCTACATTGAAAACTAAGAGGCCTCC	deletion of the PWP domain
JT1205	*SRV2*	GAAGATCTGCGGCCGCCCTCTTAGTTTTCAATGTTGATGG	deletion of the CARP domain
JT1206	*SRV2*	GAAGATCTGCGGCCGCTTAATATTGCGAGGAGCATTAATTG	deletion of the CARP domain
JT2744	*SRV2*	CTAATGCGATTGCGGCCGCGTACAGAGAGTCTGATCCTAATG	mutagenesis (*srv2-91*)
JT2745	*SRV2*	CTGTACGCGGCCGCAATCGCATTAGTCCAAAACTGTGCTGCGTCC	mutagenesis (*srv2-91*)
JT2746	*SRV2*	CCAGCAGCGGCCGCGCCTCCACCAGCCCCACCAGCTTC	mutagenesis (*srv2-201*)
JT2747	*SRV2*	TGGAGGCGCGGCCGCTGCTGGAGCCGCTGTAGCACTTG	mutagenesis (*srv2-201*)
JT2748	*SRV2*	AAGGGTGCAGCGGCCGCGGACAAATCCCAACAAACTCAC	mutagenesis (*srv2-98*)
JT2749	*SRV2*	TTTGTCCGCGGCCGCTGCACCCTTAGTGATATTTTCACCC	mutagenesis (*srv2-98*)
JT2750	*SRV2*	TCCGGTGCGGCCGCGAGGCCAAAAAAGCCATCAAC	mutagenesis (*srv2-203*)
JT2751	*SRV2*	TGGCCTCGCGGCCGCACCGGATTTACTTCCTGTGG	mutagenesis (*srv2-203*)
JT2752	*SRV2*	GTTTATAGCTAATTACGCAAATGAAACTGAATCTCTGG	mutagenesis (*srv2-104*)
JT2753	*SRV2*	TCATTTGCGTAATTAGCTATAAACCATTTGTTTCCTACC	mutagenesis (*srv2-104*)